Overview

Technology modules from micro- and nano-electronics for the life sciences

M. Birkholz,* A. Mai, C. Wenger, C. Meliani and R. Scholz

The capabilities of modern semiconductor manufacturing offer remarkable possibilities to be applied in life science research as well as for its commercialization. In this review, the technology modules available in micro- and nano-electronics are exemplarily presented for the case of 250 and 130 nm technology nodes. Preparation procedures and the different transistor types as available in complementary metal-oxide-silicon devices (CMOS) and BipolarCMOS (BiCMOS) technologies are introduced as key elements of comprehensive chip architectures. Techniques for circuit design and the elements of completely integrated bioelectronics systems are outlined. The possibility for life scientists to make use of these technology modules for their research and development projects via so-called multi-project wafer services is emphasized. Various examples from diverse fields such as (1) immobilization of biomolecules and cells on semiconductor surfaces, (2) biosensors operating by different principles such as affinity viscosimetry, impedance spectroscopy, and dielectrophoresis, (3) complete systems for human body implants and monitors for bioreactors, and (4) the combination of microelectronics with microfluidics either by chip-in-polymer integration as well as Si-based microfluidics are demonstrated from joint developments with partners from biotechnology and medicine.

How to cite this article:
WIREs Nanomed Nanobiotechnol 2016, 8:355–377. doi: 10.1002/wnan.1367

INTRODUCTION

The usage of micro- and nano-electronics in the life sciences has steadily increased over the last years.[1–6] For one reason, this development is due to the molecular nature of the mechanisms of living, for the study of which it often suffices to manipulate only a small number of molecules. This fact established a high demand for miniaturized systems acting as links between men and microbiology and led to medical and biotechnological devices enabling an increased comfort for patients, the on-line monitoring of bioprocesses and various high-throughput processes to mention only a few examples. For another reason, the demand for micro-electronics in the life sciences derives from the fact that both disciplines increasingly stronger apply nano-technological methods, such that they start to share a common set of technical equipment and tools.

Modern microelectronics relies on the elementary semiconductor silicon and the complementary metal-oxide-silicon devices (CMOS) technology. In the latter, electrons and missing electrons or holes may equally act as mobile charge carriers in CMOS. Since the introduction of integrated circuits (ICs) in 1958 and, in particular, since Moore realized the number of devices per IC to double every 1½–2 years,[7] semiconductor technology followed this rule like a self-fulfilling prophecy. Meanwhile, the number of transistors in computer ICs has reached the order of magnitude of billions and their dimensions have advanced from the micrometer into the nanometer range. The continuous shrinking of device dimensions and increase of IC performance is denoted as scaling.[8,9] Its significance

*Correspondence to: birkholz@ihp-microelectronics.com

Innovations for High Performance Microelectronics, Frankfurt (Oder), Germany

Conflict of interest: Some authors are co-inventors of patent applications as derived from the projects described.

becomes obvious from the fact that the parameters of tomorrows ICs are already defined today by the international semiconductor industry.[10]

Next to CMOS technology and scaling another direction of research and development has evolved denoted as 'More-than-Moore'.[11] It aims at introducing additional functions into ICs in order to realize new applications in consumer electronics, sensoric devices, or communication technology – to mention only a few examples. The More-than-Approach is also motivated by cost considerations. Modern CMOS fabs have recently reached the 32 and 22 nm node requiring investments for appropriate clean rooms on the order of billions of Euros that lie beyond the funding options of public research institutes.

Having worked in various projects with partners from the life sciences, it seems to the authors that the interdisciplinary dialog between both disciplines suffers from disjunctive terminology and a mutual lack of knowledge of the techniques on the other side. This review endeavors to outline the technical apparatus available in micro- and nano-electronics on a non-specialist, but specific level. The presentation will focus on the capabilities of 250 and 130 nm technologies as available at the authors' institute. It should be mentioned that a substantial body of work has been accumulated in the field of hybrid junctions from neuronal cells and semiconductor devices starting with the seminal work of Fromherz et al.[12] The following developments were reviewed in Ref 13 and important progresses on neuro-microelectronic contacts and their perspective applications as implants and neural tissue interfaces are continuously reported, e.g. Ref 14–16. The focus of this work, however, will be on the fabrication of microelectronic chips, the designs of electronic circuits and systems and their applications in biosensors and biotechnology. The authors hope that the given examples will make more transparent, what life scientists may expect from the presented micro- and nano-electronics platform and how the techniques can be applied to their research and system developments.

PREPARATION TECHNOLOGIES FOR MICROELECTRONIC CHIPS

Clean Room Processing

Microelectronic chips are produced in clean rooms categorized by the number of detectable contaminants within certain size classes. Many of them rank between class 1 and 100, which indicates either less than 35 or 3520 particles with diameter >0.5 μm per m^3, see Figure 1(a) for a view into the innovations for high performance microelectronics (IHP) clean room, in which a 130 nm pilot line is run. Wafer processing is almost fully automated in clean rooms operating on smaller technology nodes and staff presence is mainly restricted to maintenance.

The technical equipment or tools are adapted to the processing of silicon wafers with a specific diameter. At the time of writing, mostly 300 mm wafers are used in modern semiconductor technology. Previous IC generations made use of 200 mm (Figure 1(b)), 6″, 4″ wafers etc., while the next 450 mm wafer generation is currently under development. Silicon wafers are perfect single crystals exhibiting the highest ratio of crystalline perfection per EUR of all materials available. Silicon atoms constituting the wafer are arranged in the diamond crystal structure (T_h^6) having a density of $N_{Si} = 5 \times 10^{22}$ cm^{-3} at ambient conditions. Most wafers exhibit an orientation with the crystallographic ⟨0 0 1⟩ axis being perpendicular oriented to the wafer surface. Nevertheless, wafers with different orientations like ⟨1 1 1⟩ may also be processed within the same clean room; the diameter, however, is generally fixed for the set of tools available. The thickness of a 200 mm wafer amounts to 0.75 mm and is much larger than the microelectronic circuits exhibiting thicknesses between 10 and 20 μm according to the technology used.

Prior to processing the electrical conductivity σ of the wafer typically amounts to 2 Sm^{-1}, a value which lies between those of metals of about 10^7 Sm^{-1} and those of isolators on the order of 10^{-12} Sm^{-1}. Type and magnitude of conductivity may be adjusted by introducing doping elements into the Si crystal lattice. For instance, doping with group V elements such as P and As will introduce additional mobile electrons and thus enhances the conductivity with negative charge carriers, i.e. *n*-type. Doping with group III elements like boron, on the other hand, will produce a *p*-type conductive Si crystal due to excess and mobile positive charge carriers, i.e. missing electrons. Smallest amounts of dopants can vary σ by orders of magnitude. The concentration of dopants N is specified by the dimensionality of cm^{-3}. Whereas $\sigma = 3.2 \times 10^{-4}$ Sm^{-1} is valid for undoped Si, the substitution of every millionth Si by one B atom ($N_B = 5 \times 10^{16}$ cm^{-3}) causes σ to increase to 145 Sm^{-1}.

Wafer processing is started with a base doping on the order of 10^{15} cm^{-3}, while any other doping level is obtained by introducing higher concentrations of dopants on the order of 10^{16}–10^{20} cm^{-3} within selected areas. The tuning of conductivity in selected volume elements of the wafer compares to the situation in biological cells, where spatially varying pH values or concentrations of electrolytes etc. are organized by

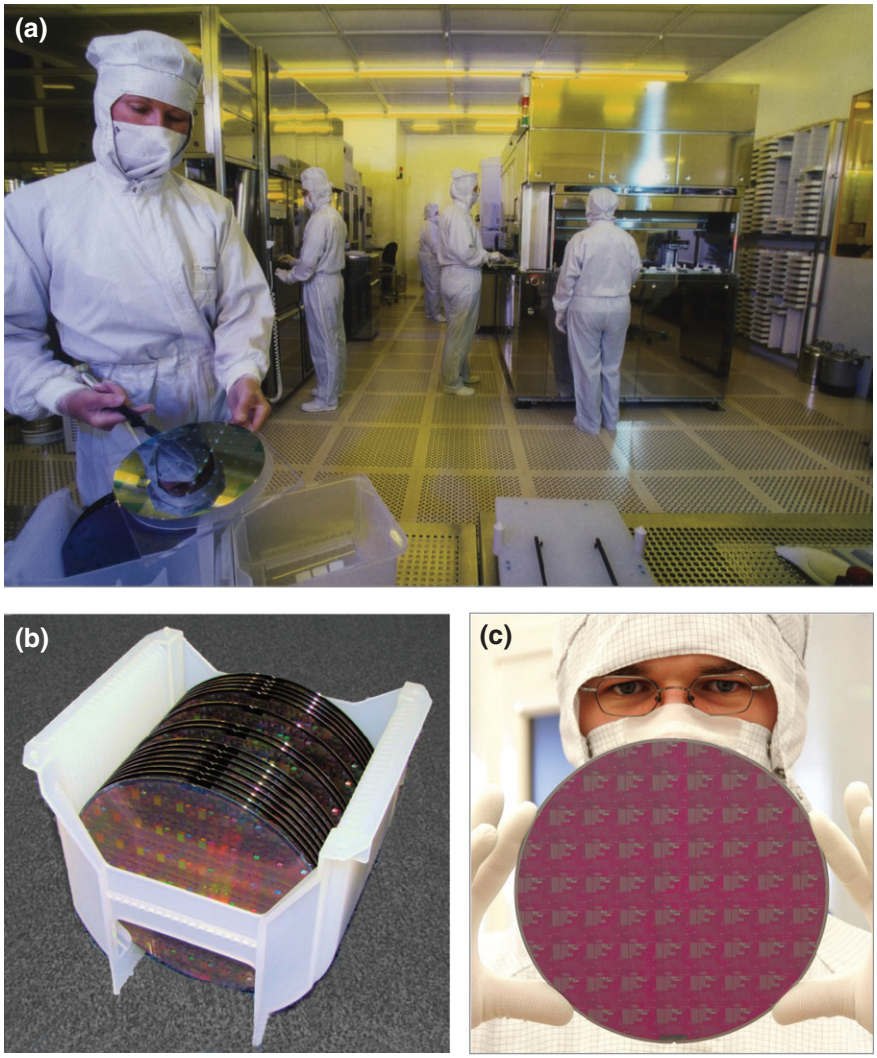

FIGURE 1 | (a) View into IHP clean room. (b) Wafer lot consisting of 24 Si Wafers having a diameter of 200 mm. (c) An almost full-processed wafer showing the separation of the surface into single dies of the same test field.

compartmenting the cell volume into cell organelles. In modern semiconductor technology doping is performed via ion implantation. Because the Si crystal lattice is severely damaged during implantation, a subsequent recrystallization is performed at high temperatures with huge heating and cooling rates up to several hundred degrees celsius per second in order to restrict possible diffusion effects.

For processing, a 200 mm wafer is partitioned in about 70–120 rectangles, so-called test fields, having a size between 10 × 26 and 16 × 26 mm (Figure 1(c)). The microchips prepared on every test field are identical so that many equal ICs are processed on one wafer. ICs are produced by a sequence of typically a few hundred process steps belonging to the groups of coating, structuring, etching, doping, and clean processes. Coatings are applied in the form of thin films having thicknesses between a few nanometer and some micrometers. The wafer is covered over its full size after depositing the coating and the small areas, from which device components such as the transistor gate or metal lines are prepared, still have to be excised. This is done by lithographic structuring and subsequent etching steps.

Figure 2 displays a cross section scanning electron microscope (SEM) micrograph of a developed and etched photoresist layer at the resolution limit accessible to the lithography tools used. The investigation aimed at implanting as small as possible *n*-doped bars in a *p*-type wafer. The photoresist coating was illuminated through a mask, in which transparent and intransparent regions alternated in order to generate stripes of light and shadow having 130 nm width. The micrograph was taken after implanting *n*-areas and prior to removal of structured photoresist and

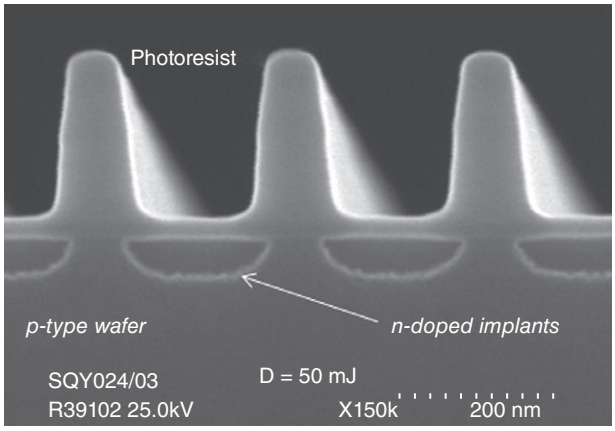

FIGURE 2 | Scanning electron microscope (SEM) micrograph of an intermediate step during the preparation of a doping lattice. The picture was taken after implantation of *n*-doped areas and prior to etching off the photoresist.

annealing.[17] Doped areas were still in an amorphous state and prone to etching, which allowed achieving a good SEM contrast. It can be seen that the intended periodicity (or pitch) of 260 nm was arrived at, albeit slight roundings of resist edges are recognized to occur. In general, the resolution achievable by photolithography determines the minimum feature dimensions of active devices that may be fabricated. The remarkable aspect of semiconductor technology is not only due to the precision achievable, but also due to the reproducibility, meaning in the example shown here that the doping bars are equably repeated more than 760,000 times along the wafer's diameter.

Transistor Types and Chip Architecture

The most important devices in microelectronic circuits are metal-oxide-semiconductor field-effect transistors or MOSFETs, which operate as amplifiers or switches. TEM micrographs of a MOSFET are given in Figure 3. Basically they act as a valve with currents flowing from the source S to the drain D, and its magnitude being controlled by the voltage applied to the gate *G*. When CMOS technology was introduced in the 1970 it was its success to allow for the complementary preparation of both *n*-channel as well as *p*-channel MOSFETs on the same wafer, where the latter are characterized by a channel current that is due to missing electrons or holes. The preparation of MOS devices requires several thin film depositions, e.g. gate oxide, polycrystalline silicon gate and source/drain spacer material and contact electrodes.

The geometrical distance between source and drain is denoted as channel length *L*. It represents a key parameter for the performance of the technology used, since it is a measure for the speed of switches that may be designed with the underlying MOSFETs. The smaller *L* is the earlier *D* is reached by charge carriers starting from *S*. Between 1975 and 2012 the channel length *L* was reduced from 3 μm to about 22 nm in modern CMOS fabs, while the clock frequency of processors increased from a few MHz into the GHz range.

An important role in semiconductor manufacturing is played by the tools for thin film deposition. The applied processes are often denoted as vapor deposition (VD), since they are usually performed via condensation from the gas phase. Two different groups may essentially be distinguished with the first one encompassing physical processes such as evaporation or sputtering, while the processes from the second group are of basically chemical nature. Depending on whether a process belongs to the first or the second group, it is either denoted a PVD or a CVD process.

For instance, the MOSFET gate from polycrystalline silicon depicted in Figure 3(b), is prepared by a CVD process, in which gaseous silane SiH_4 is introduced into the deposition chamber to decompose into Si and H_2. The wafer temperature lies between 500 and 600°C causing a thermal decomposition of SiH_4. While H_2 returns to the gas phase, the remaining Si atoms condensate on the surface to form the layer. Typical growth rates are on the order of nanometers per second.

Next to field-effect transistors FETs, where the charge carrier transport is regulated via a voltage applied to the gate, another type is represented by hetero-junction bipolar transistors HBTs. They differ from FETs by the direction of current, which is mainly oriented perpendicular to the wafer surface instead of being parallel. In addition, start and end point of the current to be amplified are named emitter and collector, with the two of them being separated by the so-called base (Figure 3(c)). Most importantly, however, the emitter–collector current is not adjusted by a voltage but by another current that is introduced laterally into the base.

While only one charge carrier type *n* or *p* is flowing from source to drain of a MOSFET, the charge transport in HBTs is related to both electron and holes that are transported in the active state and from which the notion of a bipolar device derives. Extreme high cutoff frequencies above 200 GHz may be obtained with the HBT configuration, with the base region acting as key element. It is formed from the solid binary phase $Ge_{0.2}Si_{0.8}$, with Ge atoms distributed randomly over Si crystal lattice sites. The preparation is performed as a thin layer by CVD from SiH_4 and GeH_4 by the technique of epitaxial growth, where the crystal structure of the growing film is imposed from the

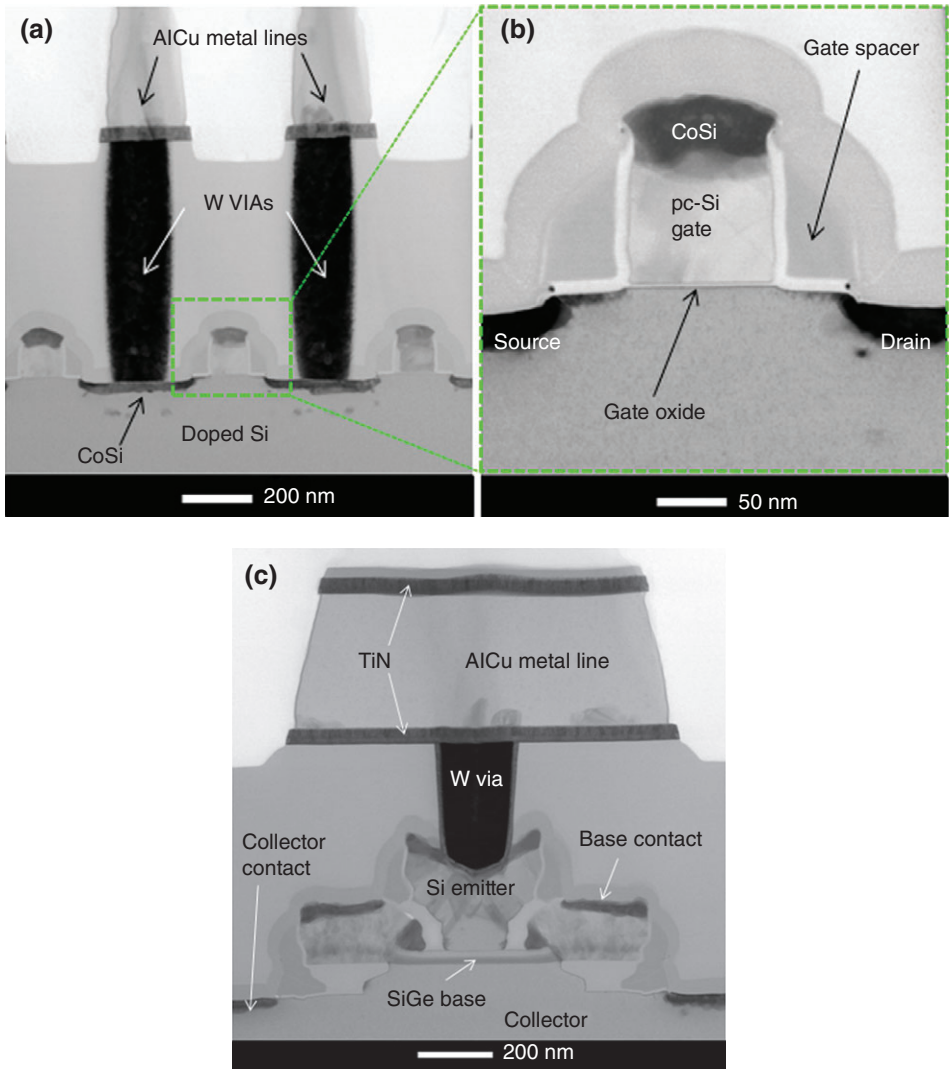

FIGURE 3 | (a) and (b) Transmission electron microscopy (TEM) micrographs of increasing magnification from the cross section of a metal–oxide–semiconductor field-effect transistor (MOSFET) having a channel length of 130 nm as routinely produced in 0.13 µm complementary metal-oxide-silicon devices (CMOS) technologies. Source and drain regions are situated directly below the vertical tungsten plugs (*W* VIAs). The thin SiO_2 film covering the channel exhibits a thickness of 2 nm. (c) TEM cross section micrograph of a most-recent hetero-junction bipolar transistor (HBT); the emitter and the base, consisting of 20 nm thin SiGe:C, have been emphasized. The electrical connection to a tungsten VIA and the lowest metal layer M1 can clearly be recognized.

underlying crystal lattice. Figure 3(c) displays the TEM micrograph of a HBT configuration. A focus of HBT research was to increase the maximum frequency of operation f_{max}, by which the device may be operated.[18] HBT limiting frequencies f_{max} of up to 500 GHz have already been achieved.[19]

Figure 4(a) displays the schematic architecture of a microelectronic chip fabricated by a 0.25 µm technology that allows for the preparation of MOSFETs having $L = 0.25$ µm. Various horizontal metal layers and vertical connections between them can be recognized that are embedded into electrically isolating glass, SiO_2, indicated by blue color. At the lower edge of the figure, active devices such as MOSFETs and HBTs can be seen that are prepared directly upon the silicon wafer. The process part used for the fabrication of active transistors is denoted as Frontend-of-Line (FEoL) and distinguished from the subsequent process parts that are named as Backend-of-Line (BEoL).

For the technologies considered horizontal metal layers are essentially made up from aluminum alloyed with a few percent of copper (Al:3%Cu). They are deposited by a magnetron sputtering process at 0.27 Pa and 200°C. Five to seven metal layers are prepared in IHP's technology flows with the precise number

depending on the technology used. The top-most layers TM1 and TM2 exhibit thicknesses of 2 and 3 μm are significantly thicker than the underlying metal layers of only 0.58 to 0.72 μm denoted by M1…M3. The latter are shown in a cross section micrograph in Figure 4(b). Also, vertical tungsten plugs may be recognized that are introduced into previously etched holes in the inter-layer dielectric (ILD). The tungsten plugs have no direct contact with Al:Cu metal layers, because the latter are covered on top and at the bottom by titanium nitride TiN, an electrically conducting ceramic acting as a diffusion barrier.

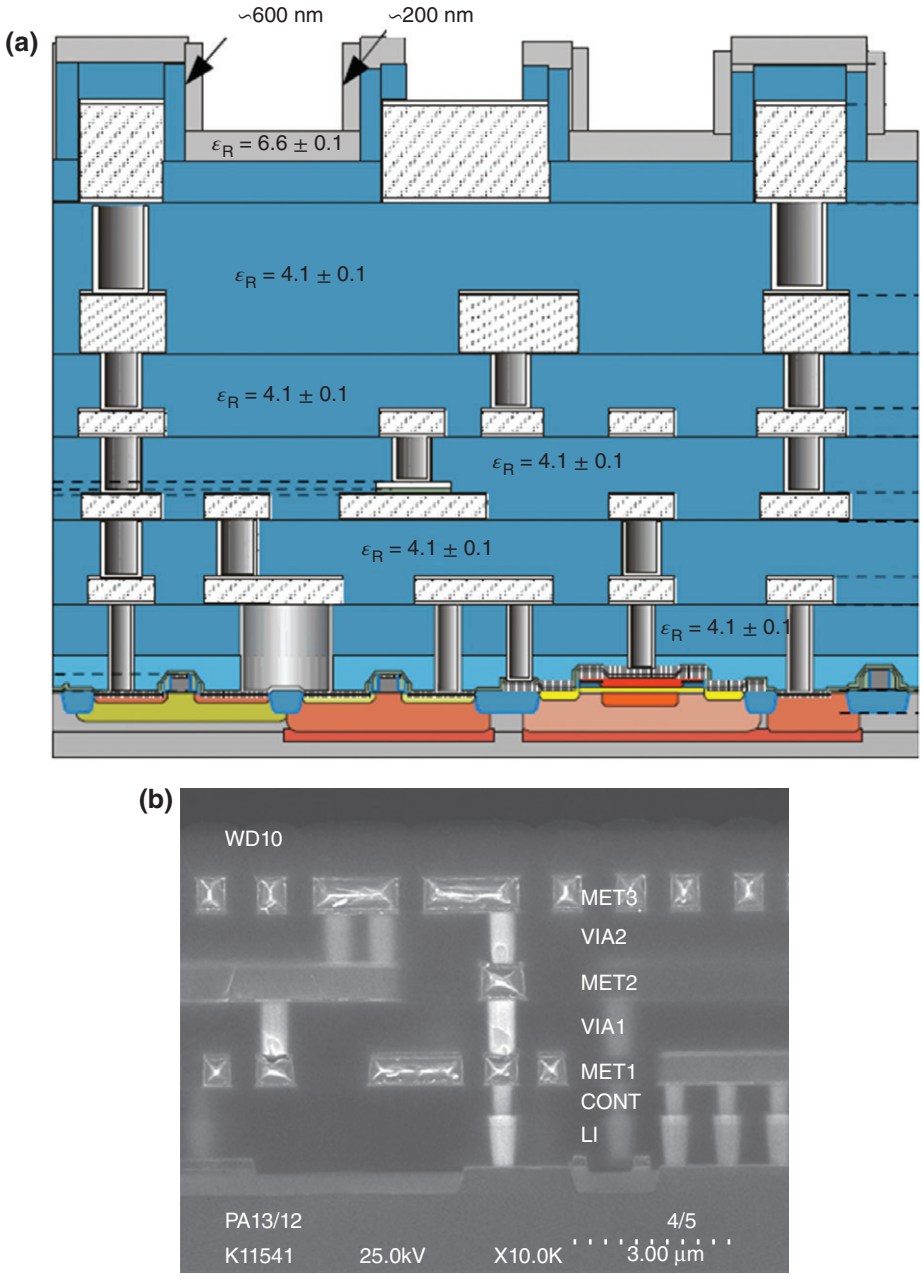

FIGURE 4 | (a) Schematic drawing of SG25H1 chip architecture in 0.25 μm technology. Blue areas are formed by inter-layer dielectric (ILD) layers that have to establish the electrical isolation between electrical connections. Metal layers M1…M3 are horizontally oriented, while vertical currents are transported by VIAs. Active devices such as *n*-type and *p*-type complementary metal-oxide-silicon devices (MOSFETs) as well as HBTs are formed directly on the Si wafer and can be seen at the bottom. The layer stack is terminated on top by a passivation layer of silicon nitride (grey) having openings only in the area of bond pads. (b) Scanning electron microscope (SEM) cross section micrograph of a chip architecture processed until to ILD3. The framing of metal layers M1 to M3 into a top and bottom TiN layer may clearly be recognized as well as the VIAs connecting them.

From the materials science point of view, TiN is a remarkable solid that behaves in mechanical respect like a ceramic and, concomitantly, disposes of an electrical conductivity of 5×10^6 Sm^{-1} comparable to those of metals.[20] TiN layers in CMOS architectures obey only a few nanometers thicknesses and are usually deposited by the PVD technique of magnetron sputtering. TiN remains practically un-corroded when brought in contact with biogenic fluids. Altogether, metal layers and W plugs act as lateral and vertical electrical connections. They are electrically isolated by embedding them in ILD. The latter are essentially formed from SiO_2 deposited by CVD techniques with SiH_4, O_2, O_3 or other gaseous precursors that are introduced into the deposition chamber and reacted at temperatures of up to 400°C on the wafer surface.

Another group of processes used in microelectronic clean rooms are etching processes. They mainly apply to selected areas of thin films deposited over the full wafer that are not required for the circuit to be configured. On the one hand, etching may be based on wet-chemical processing, where the wafer is dived into an etching solution. Well known, for instance, is the HF dip, by which the wafer is submerged for a few minutes in 2% HF in order to dissolve the native oxide SiO_2 layer that covers every elemental Si surface under ambient conditions with a thickness of 1.2 nm.

On the other hand, plasma etching techniques are moreover applied operating with ions accelerated toward the wafer in order to sputter unwanted layers off the surface. These processes may only be performed in vacuum chambers, because plasma may only be ignited under low-pressure conditions. Etching processes can be performed selectively by covering the surface with dedicated layers as e.g. photoresist and opening only over areas intended for etching.

Essentially, all processes have now been presented for fabricating microchip architectures as shown in Figure 4. Several of the structures mentioned like irradiated photoresist or etched-off layers are measured during wafer processing by SEM and other inspection techniques. Special control structures are designated for this purpose on every test field, by which, for instance, the critical dimensions of MOSFET gate lengths L, widths W, and other parameters are controlled.

In addition, various test devices are subjected to electrical control. They are denoted as process control monitors and encompass MOSFETs, HBTs and devices for determination of sheet resistances or capacitors. A complete measurement of a wafer thus yields between some thousand measurement points that are automatically valued, the results of which decide on releasing the wafer to the customer.

Surface Conditioning

An important presupposition to be fulfilled relates to the state of the particular surface that interacts with the bio-milieu.[21,22] In most cases the interaction has to act through defined material windows, because of the high corrosivity of electrolyte solutions versus semiconductors.

An illustrative example is given in Figure 5 showing an optical microscope view of the surface and a SEM cross section view of a microelectronic chip, where a defect in the surface passivation has allowed the surrounding electrolyte solution to reach the TM1 level. It may be recognized that the metal line made of Al:Cu has been damaged along a path of many micrometers causing a total failure of the sensor chip. Such defects have to be avoided without restraints and various measures can be taken for this purpose such as planarization of the surface[23] or usage of particular nitrogen-rich silicon nitride.[24]

Metallic Electrodes

In most bioelectronics devices a set of metallic electrodes has to interact electrically with the bio-milieu. This is a particular challenging task, because the presence of electrical fields was often observed to intensify

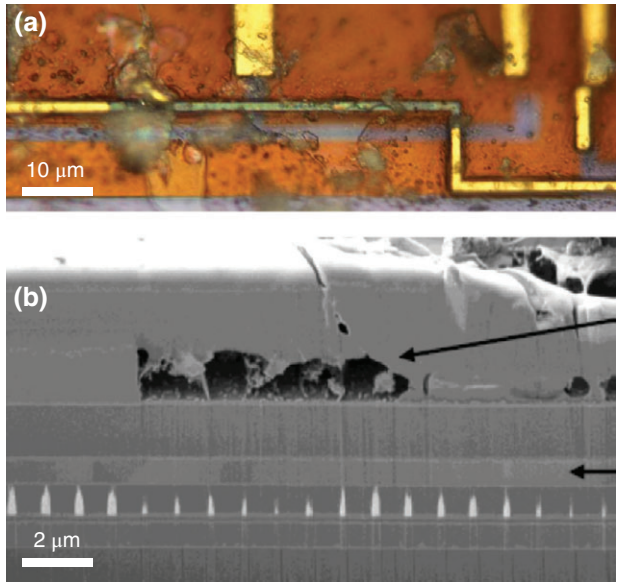

FIGURE 5 | (a) Optical microscope picture of the surface of a microchip after storing it in electrolyte solution for some days. A top-most metal layer has been subjected to corrosion as can be recognized by the color change from yellow to green. (b) Scanning electron microscope (SEM) cross section micrograph of the same area shows a penetration of the passivation layer, which turned out to be caused by the topography variation at the edge of TM1-induced surface protrusion. Such defects can be avoided by usage of an alternative passivation nitride and by a CMP step for planarization.

corrosion effects. In these situations titanium nitride may be the material of choice, as it turned out remarkably corrosion-resistant. Its corrosion-resistance in biotechnological applications is expressed by negligible redox rates in cyclic voltammograms when TiN was used as working electrodes.[25] Accordingly, TiN electrodes are applied in biomedical applications such as the artificial retina implant[21] or IHP's glucose sensor chip.[26,27] TiN should always be considered as the top-most electrode material, when the electrodes are intended to interact with bio-milieus.

Introducing other metals into the clean room than those already processed is not an easy task. This is due to the fact that various metal atoms in semiconductors act as deep recombination centers for free charge carriers. The associated reduction of current densities is detrimental to many devices and may cause their failure. Additional materials thus have to pass an extensive qualification procedure, before releasing them for preparation processes in the clean room.

The usage of some materials, however, is excluded from the outset. This holds, for instance, for gold acting as efficient recombination center in silicon. On the other hand, gold is multiply used for the immobilization of organic molecules on technical surfaces by forming a covalent bonding via sulfur atoms.[28,29] Post-CMOS processes have thus been developed that allow for the deposition of gold electrodes on otherwise fully processed microelectronic chips.[30] For this purpose, the wafer is covered with photoresist, exposed and developed and finally discharged from the clean room to receive a full-covering gold deposition outside. In a subsequent lift-off process the wafer is bathed in resist-dissolving solution leaving only the areas with an Au layer that were not covered by resist.

Nanostructured Surfaces for Immobilization

Alternative protocols may apply for the covalent immobilization of biomolecules that were initially developed for glassware, since the native SiO_2 surface layer exposes hydroxide groups Si-OH into aqueous media. Here, the well-known cross-linking techniques based on organosilanes like aminopropyl-triethoxysilane (APTS) should be considered or double cross-linking that additionally make use of glutaraldehyde (GD).[31,32]

It appears more elegant to immobilize biomolecules on semiconductor surfaces by other methods such as physical adsorption. In particular, the interesting perspective arises for microelectronics to make use of electrical fields generated within the chip itself. In principle, this approach will enable to map the structures inscribed into the silicon surface to the immobilized molecular layer.[33] A first approach for electrically assisted immobilization is offered by the structuring of a silicon surface by alternating *p*- and *n*-doped

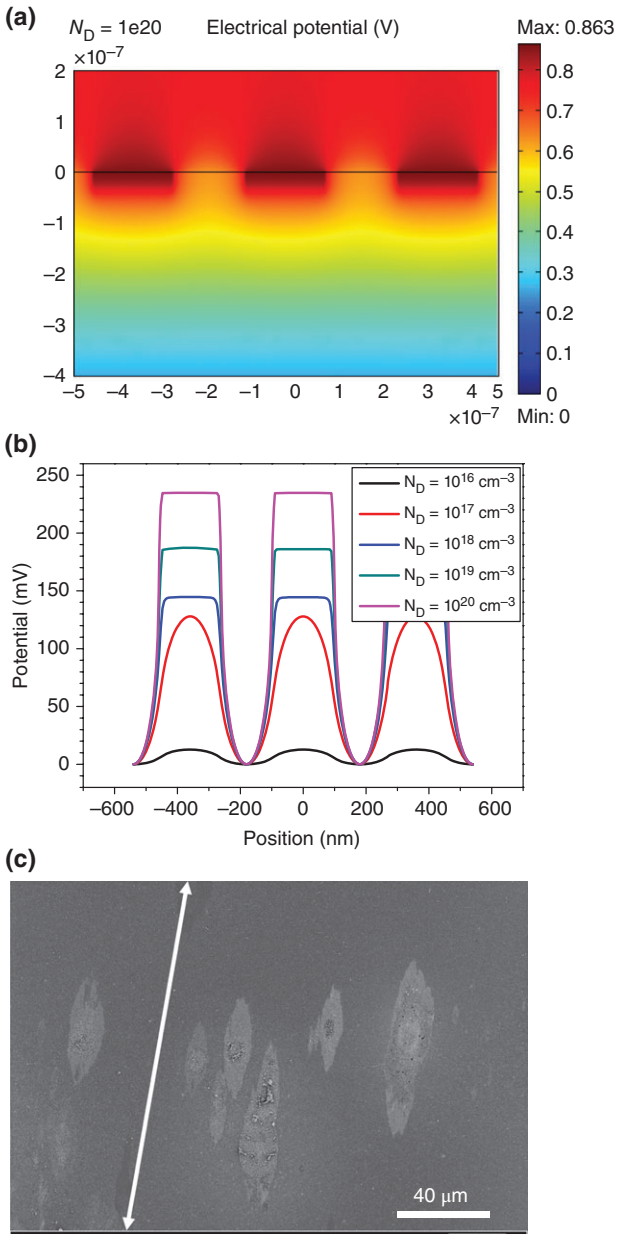

FIGURE 6 | (a) Color-scale representation of electric potential distribution in and above a doping lattice as calculated by an finite-element simulation (FEM) simulation for $N_D = 10^{20}$ cm^{-3}. (b) Course of surface potentials for the different cases of $N_D = 10^{16}$, 10^{17}, 10^{18}, 10^{19}, and 10^{20} cm^{-3}. Calculations were performed for the vacuum case,[35] which has to be modified in aqueous solutions due to shielding by electrolyte ions and water dipoles. (c) Scanning electron microscope (SEM) view on a doping lattice upon which MG 63 osteoblasts were cultivated. The orientation of cells along the direction of the lattice (white arrow) can clearly be recognized.[34]

stripes. Due to the diffusion of electrons and holes, a built-in electric field is formed – as well-known from the *pn* junction, with the electrical field lines will not confine to the silicon volume, but also extend above the wafer surface.

Figure 6(a) and (b) shows the results as obtained from a finite-element simulation (FEM) of a line lattice of *n*-doped stripes that were implanted into a *p*-doped wafer having a base doping N_A of some 10^{15} cm^{-3}. The width of the stripes amounted to 130 nm, while the depth of *n*-doped areas was adjusted by the implantation energy to 20 nm. Electrical fields are seen to extend up to 100 nm into the space above the surface,[35] where they can cause the orientation and attraction of dipolar molecules such as amino acids, proteins etc. It has to be mentioned, however, that electrical fields in aqueous solutions will cause the formation of a Helmholtz layer and thereby reducing the range of surface fields compared to the vacuum case.[36] An intermediate state during the preparation of a doping line lattice is displayed in Figure 2(c)[17,37]

Such doping lattices may not only have an orienting effect on biological macromolecules, but also on complete cells. The intentional orientation of cells is essential for biomechanics, cell biology, tissue engineering, and regenerative medicine applications.[38] The orienting effect of a surface doping lattice has been investigated in a model system for the case of human cancer cells. Figure 6(c) demonstrates the successful orientation of MG-63 osteoblasts along a doping lattice with a width of *p*- and *n*-doped stripes of 180 nm each.[34]

Various other methods for the structuring of semiconductor surfaces are possible, which all offer the advantages of semiconductor processing, i.e. to operate at the lowest level of the length scale accessible by technical means today and to be reproducible in large sample numbers. One variant of particular interest makes use of nanometer sized or micrometer sized electrodes that are embedded in an isolator. This may, for instance, be realized by configuring the tungsten VIAs in regularly ordered arrays. The preparation scheme and micrographs of such an array are shown in Figure 7 with *W* electrodes of 500 nm diameter and 2 μm distance.[39] Such arrays may effectively be used to pursue an electrical immobilization of small objects by dielectrophoresis (DEP) as shown in the next section.

BIOSENSOR MODULES

Sensor technology represents the main field of applications, to which microelectronics currently delivers the most relevant contributions to biotechnology. Firstly, this relates to the miniaturization enabled by the use of microchips for the measurement of physicochemical quantities such as temperature, pressure, conductivity, ion density, pH or viscosity etc. In addtion, microsensors are multiply applied for the detection and measurement of concentrations of biochemical analytes in samples of serum, whole blood, or cell culture media etc. The miniaturization of biosensors is of particular interest, since it paves the way for integrating it close to the point of interest or point of care and to monitor the analyte concentration regularly. The obtained transients of metabolites or other small biomolecules may be of great interest to medical research, the individual health of a patient or the understanding of a bioprocess.

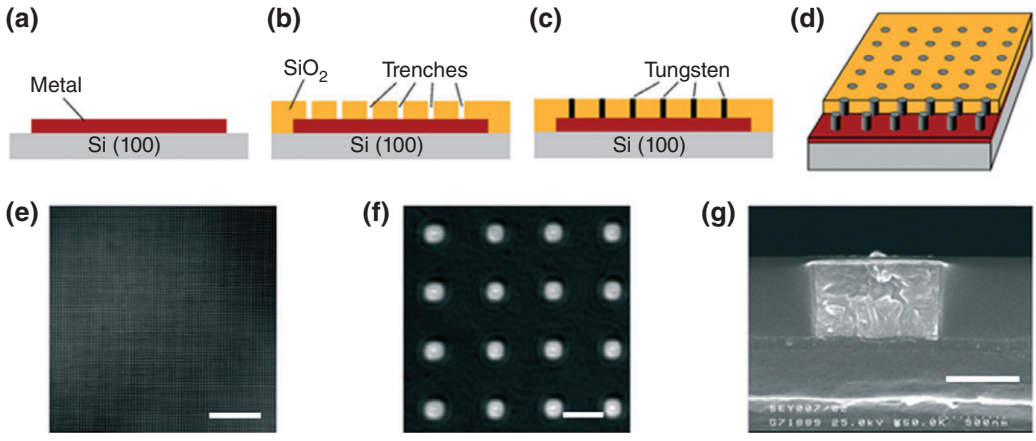

FIGURE 7 | Fabrication process of microelectrode array for dielectrophoretic immobilization: (a) metal deposition; (b) SiO_2 deposition, CMP and VIA etch; (c) tungsten filling of vias and subsequent CMP; (d) 3D side view; (e) confocal reflection microscopy of a part of the array, scale 50 μm; (f) detail view of part label e, scale 2 μm; (g) Scanning electron microscope (SEM) cross section micrograph of a single tungsten electrode with embedding SiO_2 and metal layer beneath, scale bar 500 nm.[39]

Microelectromechanical Systems (MEMS)

Also micro-electromechanical systems (MEMS), which combine microelectronics with mechanically excitable parts, have been developed for this purpose.[40,41] A microviscosimeter may serve as an example that operates by affinity sensorics to determine low-molecular weight analytes. The detection scheme relies on an assay containing a receptor and a polymer formed from analyte monomers and being spatially separated by a semipermeable membrane from the test solution. The receptor is acting as a weak antibody with a highly specific paratope for the target molecule. However, its dissociation constant K_d is only on the order of 10^{-3} …10^{-5} M and the receptor–analyte binding then is of reversible nature.

The plant lectin Concanavalin A (ConA) has been used in many investigations for glucose detection due to its specific binding pocket for glycosyl and mannosyl residues. The protein is isolated from *Canavalia ensiformis*, which was one of the first, purely isolated proteins[42] and encompasses 235 amino acids with 26.5 kDa.[43] The formation of the active tertiary structure requires the inclusion of Mn^{2+} and Ca^{2+} into the functional center and for physiological pH values ConA configures into a homo-tetramer with sugar binding sites being exposed at its periphery.

Mixing ConA with glucose polymers like dextran causes the formation of a macromolecular network between lectin tetramers and polymer molecules exhibiting a gel-like character. Mixtures with high viscosities on the order of a few 100 mPa s may be prepared by varying the size of dextran molecules, the ConA or dextran concentration.[44] The usage of such mixtures for the determination of glucose concentrations appears of having been investigated for the first time by Schultz et al.[45] Various approaches to measure glucose by affinity assays have been tested since then, which initially relied on fluorescence detection,[46–49] to later encompass impedance-based[50–52] and viscosimetric techniques.[53–57]

The variation of viscosity due to glucose variation is made use of in a recently developed variant. A BioMEMS has been developed for this purpose, in which a bendable beam is moved through the ConA-dextran-glucose assay and from the velocity of which the viscosity is deduced, see Figure 8(a). The beam is bend in a quasi-electrostatic operation mode, i.e. a high-frequency (HF) voltage is applied to attract the beam to the ground plate. The frequency amounts to 3.2 GHz and is situated between the absorption maximum of water at about 17 GHz and of protein solutions at some 100 MHz.[58]

During the measurement the beam is moved toward the ground plate and from the time t_{sw} it takes to reach a defined position the viscosity is derived. Figure 8(b)–(d) show one of the measuring chambers

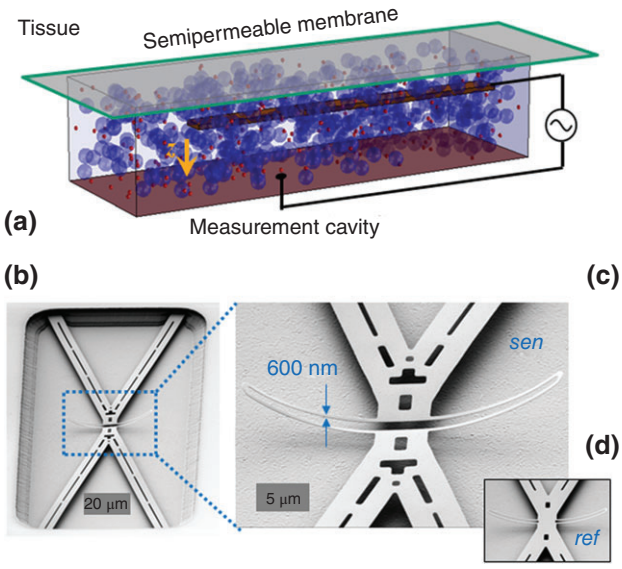

FIGURE 8 | (a) Scheme of MEMS concept and operation of an affinity sensor. A cavity is filled by the assay encompassing the receptor (small red balls) and the polymer of the analyte (large blue spheres). The network formed by macromolecular receptors and polymers partially decomposes under inserting the monomeric analyte, which leads to a change in viscosity. (b) Scanning electron microscope (SEM) picture of an assay-free MEMS with mechanically bendable beam having the shape of an X. Beam and ground plate are prepared from biostable TiN with the beam thickness amounting to 50 nm only. (c) The elastically restoring element in the middle of the beam takes the shape of an open double U. (d) The beam is formed immoveable for a parallel reference measurement by closing the double U.

realized (without the assay) and a fourfold clamped beam exhibiting a thickness of only 50 nm. The restoring mechanical element in the middle of the beam is designed in the form of a double-U. Beam and ground plate are made from TiN due to its demonstrated in vitro and in vivo stability.[23,25] Glucose may continuously be monitored with this BioMEMS in the relevant physiological range between 0.3 and 30 mM with a precision of a few percent[57] (Figure 10(c)).

Label-free Immunoassays

Microelectronics may also be applied for the classical approach of immuno-assays with very small dissociation constants K_d of the receptor–analyte complex in order to realize the detection with a miniaturized system. Again, the success is decided about by the performance of the interface, i.e. by the immobilization of antibodies on the semiconductor surface and its biocompatible design. Various sensoric techniques have been investigated for the microelectronic transformation of the binding event into an electrical quantity.

One approach makes use of DEP[59] and the tungsten arrays presented in the previous section. It was shown in Ref 60 that the functionality of anti-bodies could be conserved after their dielectrophoretic immobilization. An array as displayed in Figure 7 was applied for this purpose with all tungsten nanocylinders being subjected to the same alternating voltage by connecting them via a bottom metal layer. DEP with such an array appears particularly suited for molecules compared to cells, because their small dimensions and curvature (30 nm in the case considered here) allow for the generation of sufficiently strong electrical field gradients. Frequencies in the 10…100 kHz range turned out as optimal with respect to avoiding thermally induced effects and formation of gas bubbles. These frequencies were successfully applied for investigations carried out with intrinsically fluorescing protein R-phycoerythrin RPE that was brought in contact with mouse anti-RPE-IgG1 anti-bodies. The array was positioned under a fluorescence microscope and covered with ITO-coated glass serving as a counter electrode (Figure 9(a)). Anti-bodies were first immobilized on W electrodes by applying a 100 kHz voltage with 18 V_{rms}, which was followed by a rinsing step. Finally, REP was introduced and its binding to immobilized anti-bodies can clearly be recognized by inspecting the fluorescence micrograph (Figure 9(b)).[39]

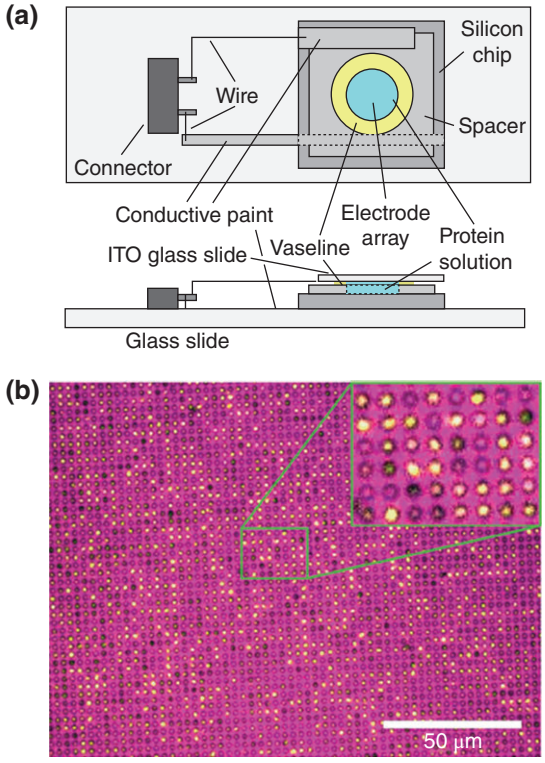

FIGURE 9 | (a) Measurement set-up for dielectrophoretic electrode array on a microscope slide (75 × 25 mm). (b) Dielectrophoretic immobilization of anti-RPE anti-bodies and subsequent incubation with RPE. An alternating voltage of 100 kHz and 18 V_{rms} has been applied for 20 min. The figure depicts the superposition of a reflection picture of the array (grey values converted to violet) and a fluorescence picture (grey values converted to yellow).

FET-derived Sensors

In addition to BioMEMS, SAWs, and MRRs the classical bio-analytical devices of microelectronics have to be mentioned, which are ion-selective field effect transistors ISFETs. Various derivatives were developed from them[61] such as ChemFET, EnzymeFETs etc., which all operate by the same principle: instead of using the gate voltage V_{SG} to tune the source-drain current of a MOSFET, an ion-sensitive or analyte–sensitive layer above the FET channel is used to modulate the channel current I_{SD}. Molecular receptors have to be immobilized upon the gate that interact with the analyte via diffusion or chemical bonding to vary I_{SD}, and from the variation of which the concentration may be deduced. ISFETs have found their main field of application for pH measurements,[62] for which the largest variation I_{SD} per pH of 59 mV per pH has been observed for Ta_2O_3 layers covering the channel.[63] The ISFET became largely acquainted to biotechnology in 2011, when IonTorrent presented their next generation sequencing tool for DNA sequencing.[64]

Spatiotemporal variations in various fields of biotechnology may be investigated by a recently developed ion camera that also operates with an ISFET array and achieving resolutions of 66 µs and 70 ms in space and time.[65] ISFETs have been adopted for the detection of alkali metal ions, penicillin in combination with pH and functional hybrid systems with living cells for both fundamental studies and biosensoric applications to mention only a few examples.[66–68]

Impedimetric Sensors

Next to classical biosensors that operate via aptamers, lectins, or enzymes by the principle of steric complementarity, the detection may also be performed by electromagnetic procedures taking a kind of finger print from the target molecules. Rather promising appears the extension of impedance spectroscopy or dielectric spectroscopy from kHz and MHz into the GHz range. Appropriate sensor structures may be prepared by semiconductor technology in a comparatively simple manner, because oscillator circuits only have to supply their output signals to interdigitated electrodes (IDE)[69–71] or microstrip lines[72] in the vicinity of the biomilieu to let them interact with the biochemical assay under investigation. The dependence on angular frequency $\omega = 2\pi f$ is accounted for by the dielectric function $\varepsilon(\omega)$, for which

the real and imaginary parts ε' and ε'' for water are shown in Figure 11(a). The course of the dielectric function of a typical protein solution is overlaid to the figure showing an additional resonance peak at about 100 MHz, i.e. at lower frequencies due to the higher mass of proteins compared to H_2O.

The analysis of impedance spectra always requires a dielectric modeling for interpreting the measured data, which recursively allows for deducing the molecules and their concentration. Compared to an enzyme test, the technique is of limited specificity and requires thorough pre-investigations with respect to the assignment of possibly occurring spectral patterns. Advantageously, impedance spectroscopy also allows for the monitoring of full cells and cell ensembles.[71]

The geometry parameters of IDE have to be adapted to the frequency range used in impedance spectroscopy. They accordingly shrink with increasing frequency. For a frequency of 12 GHz, for instance, the penetration depths of electrical fields maximally amounts to a few millimeters into a water solution for an optimally designed IDE geometry. This aspect has to be considered, whenever spatial inhomogeneities of molecules or cell densities may be expected within the solution under investigation.

The frequency range above 1 THz increasingly comes into focus of bio-analytics, but comparatively few spectroscopic studies were performed. In general, the penetration depth up to which THz sensors may gain information from biological samples is in the sub-millimeter range. The investigations performed pointed to characteristic peak patterns of nucleosides, nucleotides, saccharides, and proteins that compare to the detection specificity in UV–VIS spectroscopy.[73,74] At the moment, Si-based microelectronic circuits are still unavailable for such high frequencies and investigations have to be executed with III-V semiconductor wave generators.[73,75] This field of application may offer interesting perspectives for BiCMOS technologies including HF HBTs. So far, first studies with sub-THz radiation generated by SiGe:C HBT circuits were carried out for gas sensorics.[76]

MICROCHIPS FOR MOLECULE SENSORS AND CYTOMETRY

Next to the sensor modules that are in direct contact with the bio-milieu, a microelectronic chip encompasses additional devices and modules, which serve for the generation of excitation signals or the processing of measurement data. A comparable challenge was met by Baltes and co-workers during the development of CMOS hotplate chemical micro-sensors, which were mainly applied as gas sensors and can be regarded as early lab-on-chip systems.[77]

Figure 10(a) schematically depicts the central elements of the electrical circuits of the affinity sensor chip introduced in the previous section. A nearly mirror symmetry can be recognized to divide the upper and the lower part, which stands for the division of the circuit into a measuring MEMS (top) and a reference MEMS (bottom). The cavities of both MEMS are blue shaded and their properties are modeled in this equivalent circuit by parallel operating capacitors (C) and resistors (R). Both devices are marked by an arrow to indicate that their absolute values are varying during beam bending. This holds, however, only for the measuring MEMS and not for the reference one, because the latter is mechanically rigid and does not bend, although it is subjected to the same voltage.

A HF voltage of 3.2 GHz is applied to the beam, while the chip is powered with a DC voltage of 3 V. The required HF voltage thus has to be generated on-chip, for the purpose of which three inverters are used forming a ring-oscillator circuit. An inverter is simply build up from a p- and an n-transistor. Electrical circuits composed of an uneven number of inverters have the remarkable property to convert a DC supply into an oscillating resonance state with resonance frequency f_0 depending on the design parameters of the transistors. The capabilities of the sensor-chip with a foot print of ½ mm^2 only (Figure 10(b)) have already been demonstrated for in vitro glucose measurements (Figure 10(c)).

An important step on the way to realize a microelectronic biochip is the design of the circuit layout. Here, the design essentially is the partition of lithography masks into dark and transparent areas. Various software techniques have been developed for this purpose that all run under the title of Electronic Design Automation (EDA). The design of circuit layouts takes place in a modular fashion with modern EDA tools, i.e. in a particular technology usable elements such as C, R, MOSFETs, HBTs etc. are stored in libraries as so-called parameter cells.

Figure 11(b) shows the micrograph of an impedance measurement chip operating in the frequency range around 28 GHz.[72] Its key element is an open microstrip line probing the solution above the chip, the dielectric function of which is measured by affecting the electrical capacitance of an oscillator circuit. Such HF impedance chips may advantageously be applied for monitoring the density of biomolecules or microorganisms in culture solutions. Parameter cells from SiGe:C HBTs, MOSFETs, pc-Si resistors and MIM capacitors as well as dedicated device developments have to be combined for the circuit design and optimized

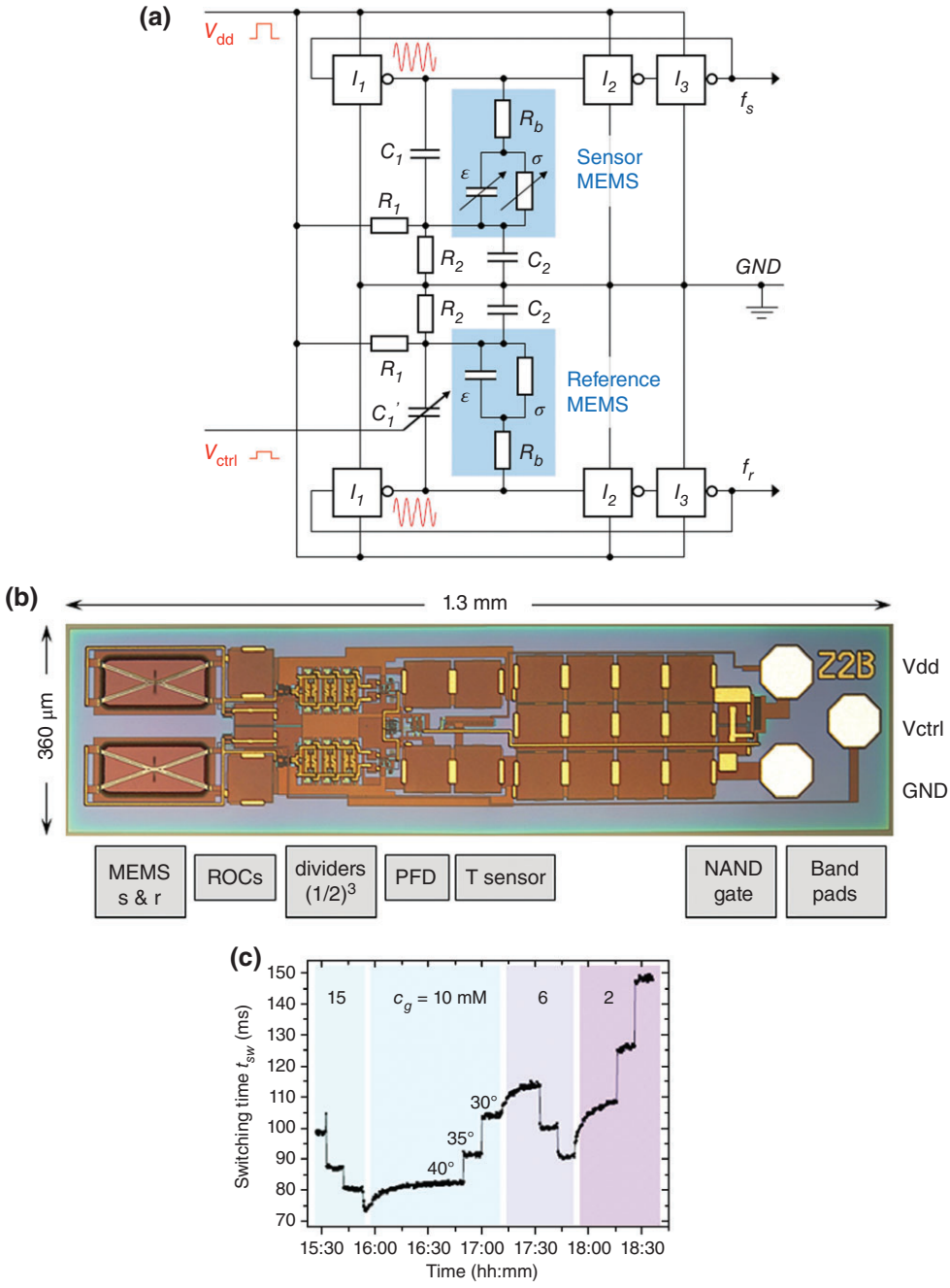

FIGURE 10 | Affinity–viscosimetric sensor chip. (a) Electrical circuit of affinity sensor chip: the DC voltage introduced is converted to a high-frequency AC voltage of 3.2 GHz via two ring oscillator circuits. The configuration of beam and ground plate acts as a capacitor *C* with serial and parallel resistors *R* (shaded areas). *C* and *R* may vary due to beam bending in the measurement circuit, which is indicated by arrows; both quantities remain constant, however, during the measurement in the reference circuit. (b) Chip photograph, from which the measurement and reference MEMS can be recognized on top and at the bottom; also the position of the different components on the chip for the signal transduction cascade are indicated. (c) Transient of the measurement parameter switching time t_{sw} for test solutions with varying glucose concentration c_g and temperature *T* as well

with respect to the intended application.[69,70,72] The chip footprint still is on the order of millimeter to allow for a sufficient spatial separation of sensor functionality in the middle of the chip and bond pads at the periphery.

The function of the designed ICs is examined by simulation runs in order to recognize possible errors prior to chip production and cost-intensive usage of clean room resources. Simulations and design optimization are often iteratively performed, until the circuit

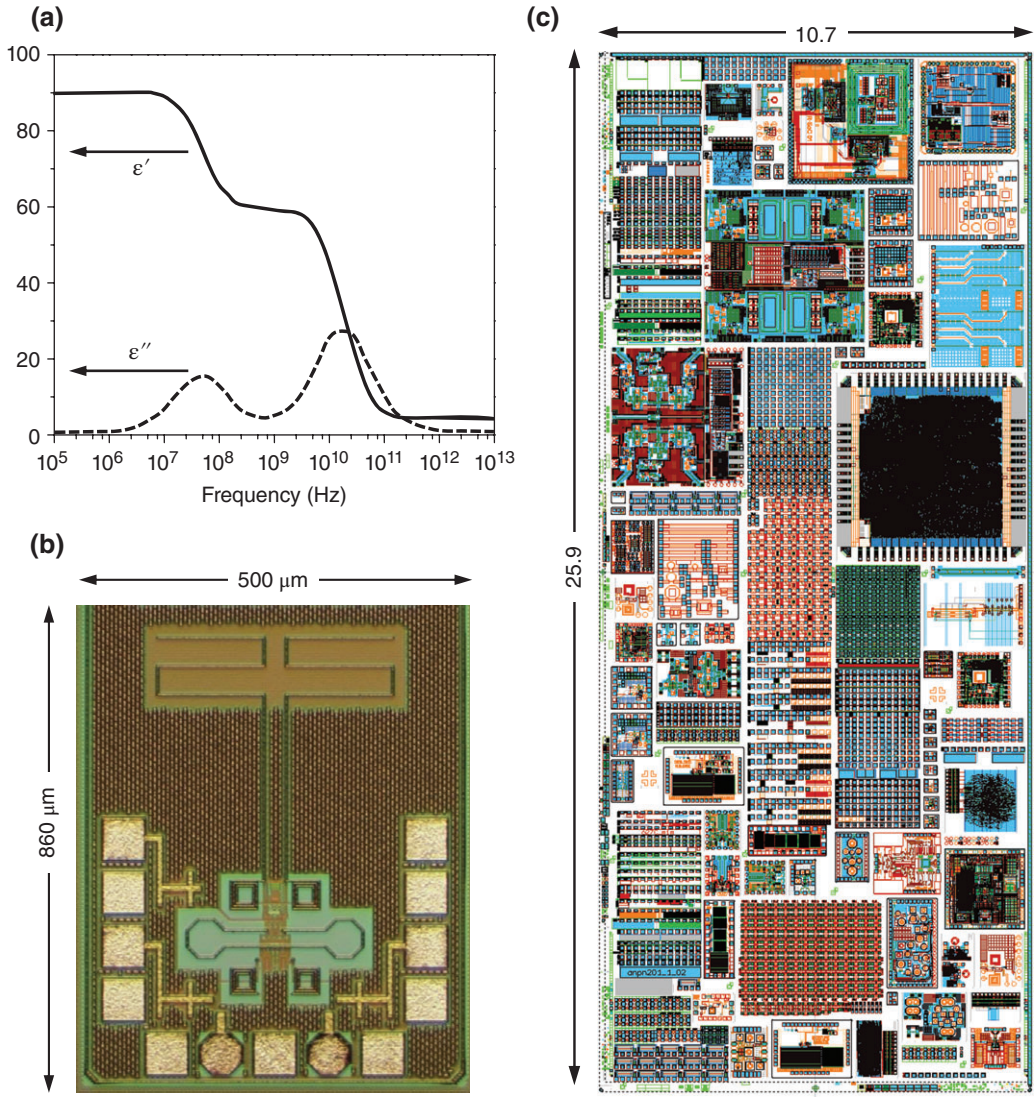

FIGURE 11 | (a) Schematic drawing of real and imaginary part ε' and ε'' of an aqueous protein solution.[58] The maximum of ε'' around 10^8 Hz is due to absorbing proteins, while the absorption maximum above 10 GHz is caused by water molecules. (b) Layout of an impedance measurement chip that can be used for the determination of cell densities. The lower part shows square-sized bond pads, while sensor elements that will come in contact with the bio-milieu are arranged on top of the chip. The distance between both was chosen rather large in order to establish a sufficient blocking of the bio-milieu and protecting the electrical contacts from corrosion. (c) Schematic overview of a test field in a 0.25 µm CMOS/BiCMOS technology occupying an area of 10.7 × 25.9 mm on a 200 mm wafer. There are about 70–120 exemplars of the same test field to be processed on each wafer of a production lot.

exhibits the intended behavior. Various constraints have to be considered during circuit design with respect to minimum distances between devices or vias or between devices and metal lines, which have been set-up to facilitate optimum chip operation. The set of geometrical constraints is denoted as design rules and a so-called design rule check (DRC) is performed for every submitted chip design. Chip preparation is generally rejected by foundries for designs failing the DRC.

Designed and simulated circuits are finally submitted to the foundry for production. After successful DRC they are included, for instance, in a full test field of an MPW shuttle. A recently processed test field in an IHP 0.25 µm MPW run is exemplarily displayed in Figure 11(c).

SYSTEM INTEGRATION

An essential development step is related to the integration of the microchip into an operative system, which must be preceded by a technical and electronic design. Also a user scenario must be defined that has to include specifications of electronic components and the system

integration and has to include the important question of sterilization.

The challenges to be expected can be illustrated by the system integration of the affinity BioMEMS presented above into a medical implant intended for a continuous monitoring of glucose levels in human tissue. The sensor is scheduled by the operation scenario to determine one glucose concentration value c_g every 5 min and to transmit the measured data five times per day. An operating time of at least half a year is planned for the sensor system. Figure 12(a) schematically depicts the implant architecture.[78]

The control of measurement cycles and intermediate data storage is usually performed by a microcontroller (μC). This is a minicomputer integrated into single chip disposing of all computer components in miniaturized form, with micro-signal processors TI MSP 430 having found the broadest dissemination. In case of a wireless data transmission the appropriate frequency band and the transmission protocol have to be chosen, by which the sensor communicates with the base station. For medical implants the 403–405 MHz frequency range has been approved by regulatory bodies,[79,80] which is denoted as Medical Implant Communication Service (MICS) and used by some 10,000 cardio implants worldwide.

System components are configured and electrically connected on a printed circuit board (PCB), which is made of highly isolating materials and exhibits only

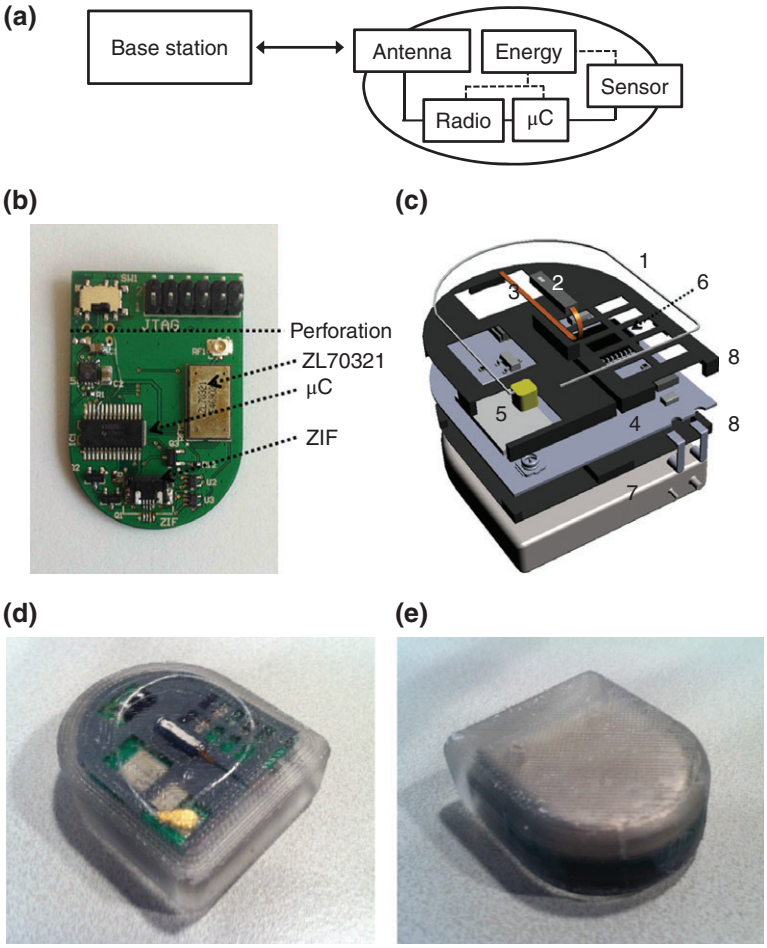

FIGURE 12 | (a) General system architecture of a bio-sensor implant. (b) Printed circuit board (PCB) of with microcontroller μC, radio module (ZL70321), and zero insertion force (ZIF) connector for connecting to sensor chip. The lateral extension of 27 mm fits to that of the battery positioned below. (c) 3D integration scheme for antenna (1), sensor probe (2), flexible cable for connecting to ZIF (3), printed circuit board (4), antenna adapter (5), microcontroller (μC) (6), battery (7), and distance holder (8). (d and e). Top and bottom view of a silicone-encapsulated biosensor implant. The sensor probe is positioned in the middle of the system in the left figure; in the picture to the right one may recognize the D-shaped battery through the silicone. The outer dimensions of the implant amount to 38.6 × 49.3 × 15.5 mm.

little absorption. Figure 12(b) shows the PCB developed for the glucose sensor implant. Electrical connections are usually implemented from copper or – for life science applications – frequently from gold. In the figure, the upper part of the PCB is seen to carry the JTAG port for μC programming, which may be cut off afterwards in order to reduce the form factor.

A battery as used in cardio implants is scheduled for the power supply[81] that has to encompass a few 100 mAh in order to enable the number of 288 measurements and 5 data transmissions per day. The battery then becomes the form-factor-determining component of the implant. Data transmission requires an antenna and the sensor chip will be connected via a so-called zero-insertion-force connector.

The BioMEMS chip was integrated into a cooling body that also allowed for the integration of the semipermeable membrane at very small distance (ca. 150 μm) above the surface of the sensor chip. It also offered sufficient space for the reception of the affinity assay encompassing Con A and dextran in an electrolyte solution. All sensor components were integrated into a full sensor system by a silicone casting,[82] see Figure 12. This system offers a platform to investigate the sensor function and stability under in vitro and in vivo conditions.

Another example relates to an autonomous sensor capsule for algae bioreactors. Goal of the project was to follow the transients of pH, electrolyte, and glucose in a photo-bioreactor build up from some 100 m of translucent tubes with an inner diameter of 5 cm. It is still unresolved, which inhomogeneities occur in such reactors and how they affect growth and yield of the algae culture.[83] Mobile capsules being transported with the fluid stream appear to be the system of choice. In this case, wireless data transmission must not obey the strict regulations of medical implants, but may follow usual industry standards.[84]

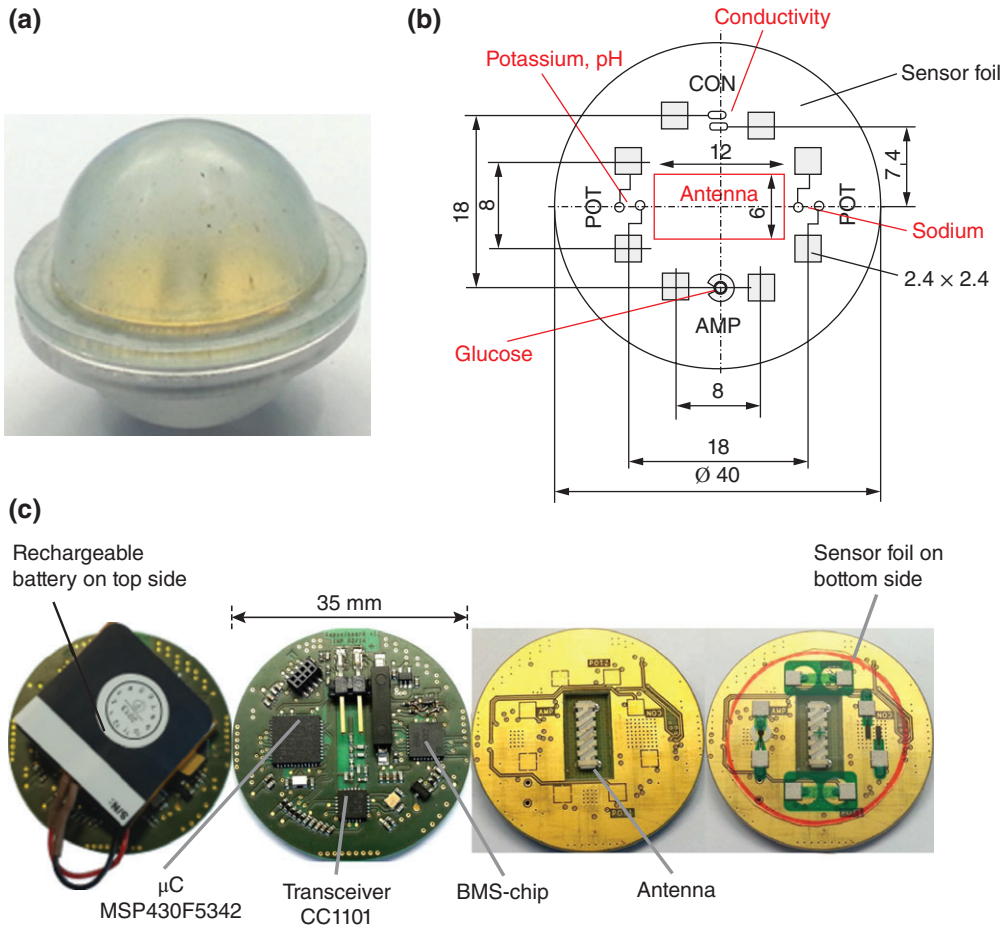

FIGURE 13 | Autonomous sensor capsule for application in photo-bioreactor with algae cultivation. (a) Outward appearance. (b) configuration of sensor surfaces on equatorially positioned printed circuit board (PCB). (c) photographs of both sides of the PCB: with microcontroller and transceiver (left) and sensor field (right). The semi-sphere above the sensor field is permeable to the cultivation broth, while the opposite side is impermeable as is the PCB layer.[85]

The outer diameter of the sensor capsule was set to 44 mm, which is a little smaller than the inner diameter of the reactor tubes.[85] The system PCB is mounted in the equatorial plane of the capsule with its upper layer exposing the sensor surfaces, while the other components of the electrical circuit were installed on the opposite side. The upper sphere of the capsule is permeable to the algae medium, while the lower part is hermetically sealed as is the PCB such that the liquid medium cannot enter the electronics-carrying side. Potentiometric sensors were scheduled for measuring pH and Na^+, while glucose was intended to be monitored by an amperometric sensor. Figure 13 schematically depicts the PCB layout, where also the electrode surface for conductivity measurements can be recognized. In this example, the transceiver CC1101 is used as radio chip operating in the 433 MHz band.[85]

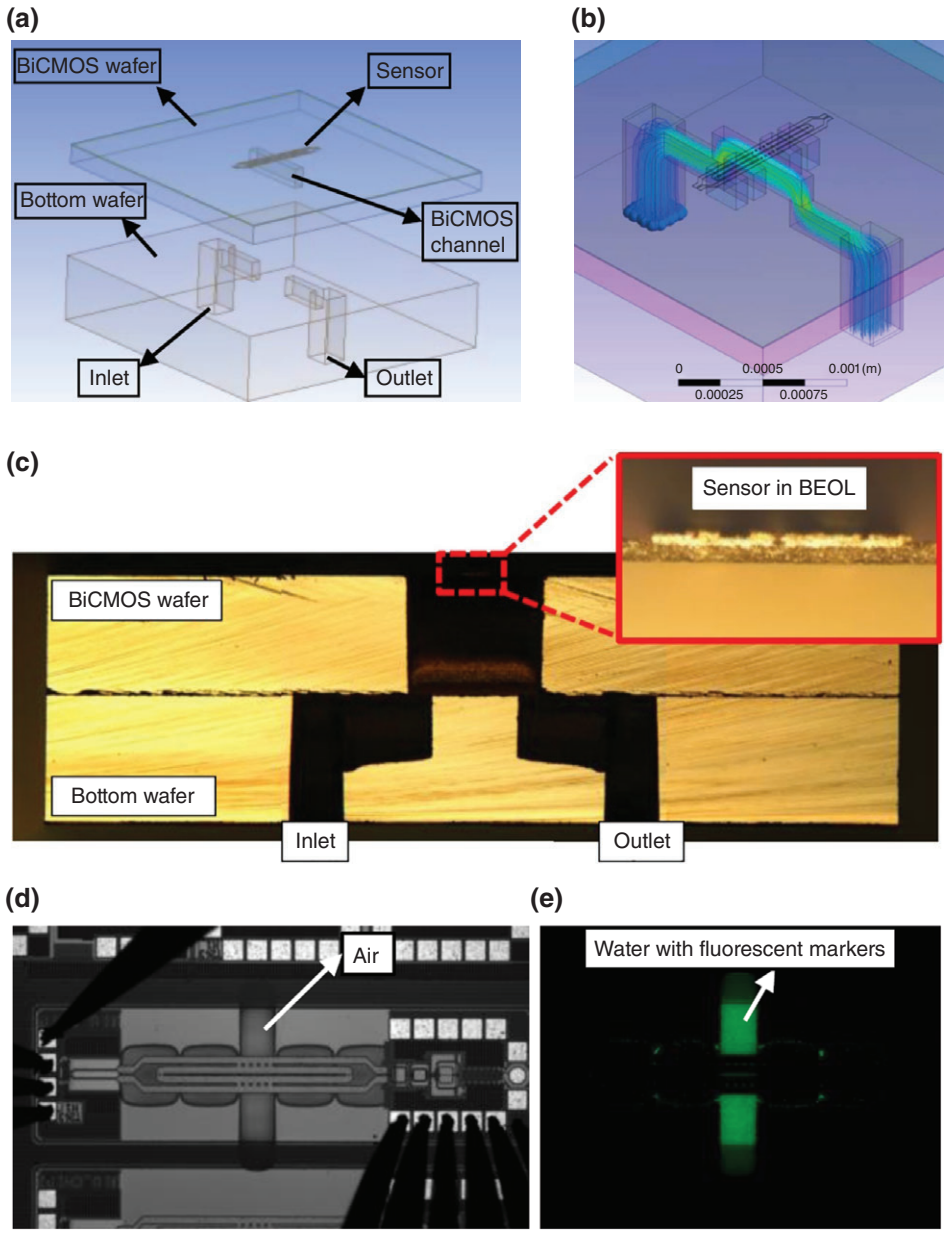

FIGURE 14 | Approach for microfluidics integration into microelectronic chips. (a) Conceptual sketch. (b) finite-element simulation (FEM) simulation of flow. (c) Cross-section micrograph of the produced wafer stack. (d) Optical microscope view on HF impedance sensor with microfluidics channel below: unfilled and (e) with fluorescence-labeled liquid.[92]

MICROFLUIDICS AND LAB-ON-CHIP SYSTEMS

Microfluidic techniques developed in the last decades offer a suitable platform for the application of microelectronics in the life sciences.[86] In principle, they may be realized from polymeric solids, while silicon was of less importance, because the access to semiconductor technology was not simple and associated with higher costs.[87] However, the perspective appears attractive to perform biotechnological experiments on combined microelectronic–microfluidic platforms and – concomitantly – the first steps of data accumulation and 'intelligent' processing. In general, the combination of both micro-techniques is a central approach to lab-on-chip technologies.

Remarkably, the first microfluidic channels were introduced in silicon wafers for chromatographic applications.[88] Today, the decisive technological process makes use of deep reactive ion etching (DRIE) and is also known as Bosch process. It can be applied for introducing the channels for fluid transport into the Si wafer and operates by a plasma-assisted etching from the gas phase. The process is capable to produce some 100 μm deep holes and ditches.[89] The common integration of fluidics and sensor elements is of particular importance for impedance spectroscopy at high frequencies, because the damping of electromagnetic radiation severely increases with increasing frequency. In particular, the objects of interest have to be very close to the sensor chip, when frequencies in the GHz range and in the THz range shall be applied for the investigation, i.e. the distance must be less than about 100 μm, with the precise value depending upon the chosen frequency, the electrode geometry and the amount of heat tolerable during the investigation.

A two wafer approach as already developed[90] may be applied to position the microfluidics in close proximity to the sensor elements of the IC.[91,92] The wafer carrying the BiCMOS circuit is thereby designated as BiCMOS wafer or top wafer, whereas the bottom wafer supplies the fluid inlet and outlet that are prepared as cylindrical holes by the DRIE process. In addition, the top wafer encompasses another microfluidic channel, which is positioned directly below the IC, by which the fluid is probed.[93] An alignment technology for backside integration was to develop in advance to allow for DRIE of the wafer backside to align the micro-channel under the sensor circuit with a precision in the 1–2 μm range.[91]

It can be seen from Figure 14 that the silicon below the sensor area is completely etched off, facilitating the fluid to stream along the bottom side of the electronic circuit. The figure also displays the stacking of top and bottom wafer in the area of the active circuit. Critical parameters are the fracture toughness of the BEoL stack and the Reynolds number of the flow in the top wafer. It is outlined in Ref 92 that flow rates of some 100 μL s^{-1} might be realized with the two-wafer configuration, even for channel heights of only 50 μm in the BiCMOS wafer.

Various projects have thus demonstrated the feasibility to integrate microelectronic circuits into microfluidic platforms. Life scientists may formulate their experimental constrains and intention to configure in cooperation with semiconductor technologists the appropriate lab-on-a-chip devices with combined components.

MULTI-PROJECT-WAFER SERVICE

In order to enable access to its technology for external users so-called multi-project wafer MPW shuttles are regularly processed at IHP (in general, such a service is offered by various semiconductor fabs). The ICs of several customers are prepared in these runs for one of the offered technologies that differ with respect to the performance parameters of MOSFETs and HBTs. Table 1 gives an overview of the technologies offered by IHP's MPW service and device characteristics.

For participation the MPW service, a potential user has to login and upload his layout data for a chosen technology run via the IHP webserver. After a formal procedure, the design rules as well the parameter cells for the most important devices will be supplied allowing for the design of customer-specific circuits. Generally, these tools have to be applied by scientists and developers from the electronic disciplines. Life scientists with interest in biochips are thus recommended to cooperate with circuit designers.

Submitted designs are combined into a common test field, which also comprises several hundred test structures and alignment markers, see Figure 11(c). After this the set of lithography masks may be prepared. Prior to clean room processing the appropriate wafer type has to be selected, whereas for product flows typically wafers with 2 Sm^{-1} and ⟨0 0 1⟩ orientation are chosen. Wafers are collected into a lot that usually comprises of 24 pieces, see Figure 1(b). Processing starts with the labelling of each wafer, which is followed by various cleaning steps. Subsequently, the essential set-up of the IC begins. It is divided into different modules such as TRENCH, TRCHFI, BLAYER etc., which stands for the separation of active areas, preparation of buried layers, and so on.

Wafer processing is finished for 0.25 and 0.13 μm technologies about 2½–3 months after starting the lot

TABLE 1 | Overview of the Technologies Offered by IHP's MPW Service and Device Characteristics

SG25H1	High-performance 0.25 μm technology with *npn*-HBTs up to f_T/f_{max} = 180/220 GHz (compare Figure 4(a))
SG25H3	0.25 μm technology with a set of *npn*-HBTs ranging from a higher RF performance (f_T/f_{max} = 110/180 GHz) to higher breakdown voltages up to 7 V
SGB25V	Cost-effective technology with a set of *npn*-HBTs up to a breakdown voltage of 7 V
SG13S	High-performance 0.13 μm BiCMOS with *npn*-HBTs up to f_T/f_{max} = 250/300 GHz, with 3.3 V I/O CMOS and 1.2 V logic CMOS
SG13G2	0.13 μm BiCMOS technology with the same device portfolio as SG13S, but much higher bipolar performance with f_T/f_{max} = 300/500 GHz

BiCMOS, BipolarCMOS; CMOS, complementary metal-oxide-silicon devices.

and after a few 100 process steps. Chips then have to be separated, which is usually performed by automated circular-blade saws. Beforehand, the wafer is subjected to thinning to reduce its original thickness to 300 μm or another customer-specified value. Next to conventional sawing the technique of laser dicing may be applied for chip separation,[94] which practically avoids any particle generation. Finally, the separated microchips are delivered for experimentation or system integration.

CONCLUSIONS

Next to micro- and nano-electronics no other technology exists that operates on length scales so close to the molecular structures of living. New bio-analytical and bio-sensor principles are enabled by them that may directly be integrated into microelectronic chips allowing for the detection, transduction, analysis, and otherwise intelligent processing of measured data within smallest regions of space. Various semiconductor fabs offer their assistance to life scientists for the fabrication of BioASICs by usage of multi-project wafer services. The pilot line of IHP disposes of a set of 0.25 and 0.13 μm CMOS/BiCMOS enabling, for instance, the preparation of MEMS devices with mechanical membranes from bio-stable TiN, di-electrophoretic electrode arrays, impedimetric measurement chips in the GHz range, HBTs with transient frequencies in the few 100 GHz range and Si-integrated microfluidics to mention only a few technology modules, from which full bio-systems might be configured. The usage of microelectronic techniques is expected to pave the way for substantial progress in various fields of life science research and development. It still suffers from the so-far disjunctive terminology between both disciplines, but the authors hope that the presented review might foster a broader utilization of microelectronics by life scientists.

ACKNOWLEDGEMENTS

We thank our colleagues from IHP that helped during the collection of this overview and which enabled to offer the technology modules presented above to external customers. We likewise thank our partners that participated in project translation and the German Federal Ministry of Research and Technology (grant numbers 0313862B and 16SV3934), German Federal Ministry of Economics (KF 0653901 UL8), the European Regional Development Fund and the German state Brandenburg (TeraSens project) for funding cooperation projects, the results of which were presented here. We particularly thank Aktionszentrum BioTOP, the diagnostic network Berlin-Brandenburg, IGE from TU Berlin and the center for molecular diagnostics and biotechnology ZMDB for long-standing and manifold support in transferring microelectronics to the life sciences, and last, but not least, the Chair of Bioprocess Engineering of TU Berlin, with which the Joint Lab Bioelectronics IHP/TUB was founded in 2012.

REFERENCES

1. Cumming DRS. ISFET technology for multi-sensor technology: from lab-in-a-pill to massively parallel measurements. *Electron Lett* 2011, 47:14–16.
2. Graham AHD, Robbins J, Bowen CR, Taylor J. Commercialisation of CMOS integrated circuit technology in multi-electrode arrays for neuroscience and cell-based biosensors. *Sensors* 2011, 11:4943–4971.
3. Rothe J, Lewandowska MK, Heer F, Frey O, Hierlemann A. Multi-target electrochemical biosensing enabled by integrated CMOS electronics. *J Micromech Microeng* 2011, 21:054010.
4. Pan T, Wang W. From cleanroom to desktop: emerging micro-nanofabrication technology for biomedical applications. *Ann Biomed Eng* 2011, 39:600–620.

5. Kumar S, Prakash R, Chouhan S, Salhan AK. CMOS sensors for microscopy, spectrophotometry and as a transducer in biosensors. In: *Point-of-Care Healthcare Technologies (PHT)*. Bangalore: IEEE; 2013, 196–199.
6. Ghallab YH, Ismail Y. CMOS based lab-on-a-chip: applications, challenges and future trends. *IEEE Circ Syst Mag* 2014, 14:27–47.
7. Moore GE. Cramming more components onto integrated circuits. *Electronics* 1965, 38:114–117.
8. Dennard RH, Gaensslen FH, Yu H-N, Rideout VL, Bassous E, LeBlanc A. Design of ion-implanted MOSFETs with very small physical dimensions. *IEEE J Solid-State Circ* 1974, 9:256–268.
9. Bohr M. A 30 years retrospective on Dennard's MOSFET scaling paper. *IEEE Solid State Circ Soc News* 2007, 12:11–13.
10. ITRS Executive Committee. 2013 edition – executive summary. *Int Technol Roadmap Semicond* 2013; 17. Available at: http://www.itrs.net/Links/2013ITRS/2013Chapters/2013ExecutiveSummary.pdf.
11. Arden W, Brillouët M, Cogez P, Graef M, Huizing B, Mahnkopf R. *More-than-Moore – White Paper*. ITRS; 2011.
12. Fromherz P, Offenhausser A, Vetter T, Weis J. A neuron-silicon junction: a Retzius cell of the leech on an insulated-gate field-effect transistor. *Science* 1991, 252:1290–1293.
13. Fromherz P. Joining microelectronics and microionics: nerve cells and brain tissue on semiconductor chips. *Solid-State Electron* 2008, 52:1364–1373.
14. Panaitov G, Thiery S, Hofmann B, Offenhäusser A. Fabrication of gold micro-spine structures for improvement of cell/device adhesion. *Microelectron Eng* 2011, 88:1840–1844.
15. Schuettler M, Donaldson N, Seetohul V, Taylor J. Fibre-selective recording from the peripheral nerves of frogs using a multi-electrode cuff. *J Neural Eng* 2013, 10:036016.
16. Ballini M, Muller J, Livi P, Yihui C, Frey U, Stettler A, Shadmani A, Viswam V, Lloyd Jones I, Jackel D, et al. A 1024-channel CMOS microelectrode array with 26,400 electrodes for recording and stimulation of electrogenic cells in vitro. *IEEE J Solid-State Circ* 2014, 49:2705–2719.
17. Birkholz M, Zaumseil P, Bauer J, Bolze D, Weidner G. Small-angle X-ray reciprocal space mapping of surface relief gratings. *Mater Sci Eng C* 2007, 27:1154–1157.
18. Osten HJ, Lippert G, Knoll D, Barth R, Heinemann B, Rucker H, Schley P. The effect of carbon incorporation on SiGe heterobipolar transistor performance and process margin. In: *International Electron Devices Meeting Technical Digest, 1997. IEDM '97*. Washington, DC: IEEE; 1997, 803–806.
19. Heinemann B, Barth R, Bolze D, Drews J, Fischer GG, Fox A, Fursenko O, Grabolla T, Haak U, Knoll D, et al. SiGe HBT technology with fT/fmax of 300 GHz/500 GHz and 2.0 ps CML, gate delay. In: *International Electron Devices Meeting (IEDM)*, Vol. 30. San Francisco, CA: IEEE; 2010, 30:1–4.
20. Martienssen W, Warlimont H, eds. *Handbook of Condensed Matter and Materials Data*. Berlin: Springer; 2005, 1120.
21. Hämmerle H, Kobuch K, Kohler K, Nisch W, Sachs H, Stelzle M. Biostability of micro-photodiode arrays for subretinal implantation. *Biomaterials* 2002, 23:797–804.
22. Graham AHD, Bowen CR, Taylor J, Robbins J. Neuronal cell biocompatibility and adhesion to modified CMOS electrodes. *Biomed Microdev* 2009, 11:1091–1101.
23. Fröhlich M, Birkholz M, Ehwald K-E, Kulse P, Fursenko O, Katzer J. Biostability of an implantable glucose sensor chip. *IOP Conf Ser: Mater Sci Eng* 2012, 41:012022.
24. Lisker M, Trusch A, Krüger A, Fraschke M, Tillack B, Weimann N, Ostermay I, Krüger O. Silicon nitride stop layer in back-end-of-line planarization for wafer bonding application. *International Conference on Planarization/CMP Technology (ICPT)*. Kobe: IEEE; 2014, 109–115.
25. Birkholz M, Ehwald K-E, Wolansky D, Costina I, Baristiran-Kaynak C, Fröhlich M, Beyer H, Kapp A, Lisdat F. Corrosion-resistant metal layers from a CMOS process for bioelectronic applications. *Surf Coat Technol* 2010, 204:2055–2059.
26. Birkholz M, Ehwald K-E, Kulse P, Drews J, Fröhlich M, Haak U, Kaynak M, Matthus E, Schulz K, Wolansky D. Ultrathin TiN membranes as a technology platform for CMOS-integrated MEMS and BioMEMS devices. *Adv Funct Mater* 2011, 21:1652–1656.
27. Kulse P, Birkholz M, Ehwald K-E, Bauer J, Drews J, Haak U, Höppner W, Katzer J, Schulz K, Wolansky D. Fabrication of MEMS actuators from the BEOL of a 0.25 μm BiCMOS technology platform. *Microelectron Eng* 2012, 97:276–279.
28. Hrapovic S, Liu Y, Enright G, Bensebaa F, Luong JHT. New strategy for preparing thin gold films on modified glass surfaces by electroless deposition. *Langmuir* 2003, 19:3958–3965.
29. Lee JM, Park HK, Jung Y, Kim JK, Jung SO, Chung BH. Direct immobilization of protein G variants with various numbers of cysteine residues on a gold surface. *Anal Chem* 2007, 79:2680–2687.
30. Kitzmann J. Strukturierte Goldabscheidung mittels Galvanik und PVD. Diploma thesis, TH Wildau. 2011.
31. Schnyder B, Kötz R, Alliata D, Facci P. Comparison of the self-chemisorption of azurin on gold and on functionalized oxide surfaces. *Surf Interface Anal* 2002, 34:40–44.
32. Birkholz M, Zaumseil P, Kittler M, Wallat I, Heyn MP. Structure of biomembrane-on-silicon hybrids derived

from X-ray reflectometry. *Mater Sci Eng B* 2006, 134:125–129.

33. Birkholz M. A thin film approach to protein crystallography. *Nucl Instr Meth Phys B* 2009, 268:414–419.
34. Körtge A, Stählke S, Lange R, Birkholz M, Fraschke M, Schulz K, Nebe B, Elter P. Alignment of MG-63 osteoblasts on fibronectin-coated phosphorous doping lattices in silicon. *World Acad Sci Eng Technol* 2013, 73:801–804.
35. Ratzke M. Kraftmikroskopie als Werkzeug zur Charakterisierung elektrischer Oberflächeneigenschaften. Doctoral thesis, BTU Cottbus, Germany, 2011.
36. Israelachvili J. *Intermolecular and Surface Forces*. 2nd ed. Amsterdam: Academic Press; 1991.
37. Zaumseil P, Birkholz M, Weidner G. X-ray characterization of periodic sub-nm surface relief gratings. *Phys Stat Sol A* 2007, 204:2657–2661.
38. Li Y, Huang G, Zhang X, Wang L, Du Y, Lu TJ, Xu F. Engineering cell alignment in vitro. *Biotechnol Adv* 2014, 32:347–365.
39. Otto S, Kaletta UC, Bier F, Wenger C, Hölzel R. Dielectrophoretic immobilisation of antibodies on microelectrode arrays. *Lab Chip* 2014, 14:998–1004.
40. Bashir R. BioMEMS: state-of-the-art in detection, opportunities and prospects. *Adv Drug Deliv Rev* 2004, 56:1565–1586.
41. Grayson ACR, Shawgo RS, Johnson AM, Flynn NT, Li Y, Cima MJ, Langer RS. A BioMEMS review: MEMS technology for physiologically integrated devices. *Proc IEEE* 2004, 92:6–21.
42. Sumner JB, Gralén N, Eriksson-Quensel I-B. The molecular weights of concanavalin, concanavalin A and concanavalin B. *J Biol Chem* 1938, 125:45–48.
43. Bouckaert J, Dewallef Y, Poortmans F, Wyns L, Loris R. The structural features of concanavalin A governing non-proline peptide isomerization. *J Biol Chem* 2000, 275:19778–19787.
44. Ehwald R, Ballerstadt R, Dautzenberg H. Viscosimetric affinity assay. *Anal Biochem* 1996, 234:1–8.
45. Schultz JS, Sims G. Affinity sensors for individual metabolites. *Biotechnol Bioeng Sympos* 1979, 9:65–71.
46. Schultz JS, Mansouri S, Goldstein IJ. Affinity sensor: a new technique for developing implantable sensors for glucose and other metabolites. *Diabetes Care* 1982, 5:245–253.
47. Ballerstadt R, Evans C, Gowda A, McNichols R. Fiber-coupled fluorescence affinity sensor for 3-day in vivo glucose sensing. *J Diabetes Sci Technol* 2007, 1:218–227.
48. Nielsen JK, Christiansen JS, Kristensen JS, Toft HO, Hansen LL, Aasmul S, Gregorius K. Clinical evaluation of a transcutaneous interrogated fluorescence lifetime-based microsensor for continuous glucose reading. *J Diabetes Sci Technol* 2009, 3:98–109.
49. Dutt-Ballerstadt R, Evans C, Pillai AP, Orzeck E, Drabek R, Gowda A, McNichols R. A human pilot study of the fluorescence affinity sensor for continuous glucose monitoring in diabetes. *J Diabetes Sci Technol* 2012, 6:362–370.
50. Huang X, Siqi L, Schultz J, Qian W, Lin Q. A capacitive MEMS viscometric sensor for affinity detection of glucose. *J Microelectromech Syst* 2009, 18:1246–1254.
51. Huang X, Li S, Schultz JS, Wang Q, Lin Q. A dielectric affinity microbiosensor. *Appl Phys Lett* 2010, 96:033701.
52. Xian H, Siqi L, Davis E, Dachao L, Qian W, Qiao L. A MEMS dielectric affinity glucose biosensor. *J Microelectromech Syst* 2014, 23:14–20.
53. Ballerstädt R, Ehwald R. Suitability of aqueous dispersions of dextran and concanavalin A for glucose sensing in different variants of the affinity sensor. *Biosens Bioelectr* 1994, 9:557–567.
54. Beyer U, Schäfer D, Thomas A, Aulich H, Haueter U, Reihl B, Ehwald R. Recording of subcutaneous glucose dynamics by a viscosimetric affinity sensor. *Diabetology* 2001, 44:416–423.
55. Zhao Y, Li S, Davidson A, Yang B, Wang Q, Lin Q. A MEMS viscosimetric sensor for continuous glucose monitoring. *J Micromech Microeng* 2007, 17:2528–2537.
56. Birkholz M, Ehwald K-E, Ehwald R, Kaynak M, Borngräber J, Drews J, Haak U, Klatt J, Matthus E, Schoof G, et al. Mikroviskosimeter zur kontinuierlichen Glucosemessung bei Diabetes mellitus. *Mikrosystemtechnik Kongress* 2009, 2009:124–125.
57. Birkholz M, Ehwald K-E, Basmer T, Reich C, Kulse P, Drews J, Genschow D, Haak U, Marschmeyer S, Matthus E, et al. Sensing glucose concentrations at GHz frequencies with a fully embedded BioMEMS. *J Appl Phys* 2013, 113:244904.
58. Gabriel G, Gabriel S, Grant EH, Halstead BSJ, Mingos DMP. Dielectric parameters relevant to microwave dielectric loss. *Chem Soc Rev* 1998, 27:213–223.
59. Pethig R. Review article – dielectrophoresis: status of the theory, technology, and applications. *Biomicrofluidics* 2010, 4:022811.
60. Laux EM, Wenger C, Kaletta UC, Bier FF, Hoelzel R. Functionality of dielectrophoretically immobilized enzyme molecules. *Electrophoresis* 2014, 35:459.
61. Schöning MJ, Poghossian A. Bio FEDs (field-effect devices): state-of-the-art and new directions. *Electroanalysis* 2006, 18:1893–1900.
62. Hammond PA, Ali D, Cumming DRS. Design of a single-chip pH sensor using a conventional 0.6-μm CMOS process. *IEEE Sens J* 2004, 4:706–712.
63. Grattarola M, Massobrio G. *Bioelectronics Handbook: MOSFETs, Biosensors, and Neurons*. New York: McGraw-Hill; 1998.

64. Rothberg JM, Hinz W, Rearick TM, Schultz J, Mileski W, Davey M, Leamon JH, Johnson K, Milgrew MJ, Edwards M, et al. An integrated semiconductor device enabling non-optical genome sequencing. *Nature* 2011, 475:348–352.

65. Nemeth B, Symes MD, Boulay AG, Busche C, Cooper GJT, Cumming DRS, Cronin L. Real-time ion-flux imaging in the growth of micrometer-scale structures and membranes. *Adv Mater* 2012, 24:1238–1242.

66. Schöning MJ, Sauke M, Steffen A, Marso M, Kordos P, Lüth H, Kauffmann F, Erbach R, Hoffmann B. Ion-sensitive field-effect transistors with ultrathin Langmuir-Blodgett membranes. *Sens Actuators B* 1995, 27:325–328.

67. Poghossian A, Schöning MJ. Chapter 14 'High-order' hybrid FET module for (bio)chemical and physical sensing. In: Alegret S, ed. *Comprehensive Analytical Chemistry*, vol. 39. Elsevier; 2003, 587–623.

68. Poghossian A, Ingebrandt S, Offenhäusser A, Schöning MJ. Field-effect devices for detecting cellular signals. *Semin Cell Dev Biol* 2009, 20:41–48.

69. Guha S, Jamal FI, Schmalz K, Wenger C, Meliani C. CMOS lab on a chip device for dielectric characterization of cell suspensions based on a 6 GHz oscillator. In: *European Microwave Conference, European Microwave Week 2013, (EuMW 2013)*. Nürnberg, 2013.

70. Guha S, Jamal FI, Schmalz K, Wenger C, Meliani C. An 8 GHz CMOS near field bio-sensor array for imaging spatial permittivity distribution of biomaterials. In: *International Microwave Symposium (IMS 2014)*. Tampa, FL: IEEE; 2014.

71. Couniot N, Afzalian A, Van Overstraeten-Schlögel N, Francis LA, Flandre D. Capacitive biosensing of bacterial cells: analytical model and numerical simulations. *Sens Actuators B* 2015, 211:428–438.

72. Jamal FI, Guha S, Meliani C. A SiGe BiCMOS dielectric sensor utilizing an open-ended microstrip line in a 28 GHz Colpitts oscillator. In: *European Microwave Week (EuMW)*. Rome: IEEE; 2014, 1032–1035.

73. J-i N, Sasaki T, Suto K, Tanabe T, Saito K, Yamada T, Kimura T. THz transmittance measurements of nucleobases and related molecules in the 0.4- to 5.8-THz region using a GaP THz wave generator. *Opt Commun* 2005, 246:229–239.

74. Saha SC, Grant JP, Ma Y, Khalid A, Hong F, Cumming DRS. Application of terahertz spectroscopy to the characterization of biological samples using birefringence silicon grating. *J Biomed Opt* 2012, 17:0670061–0670065.

75. Wolf A. Aufbau und Funktionsweise eines kontinuierlich-strahlenden Terahertz-Spektrometers. Bachelor thesis, TH Wildau, 2014.

76. Schmalz K, Mao Y, Borngräber J, Neumaier P, Hübers HW. Tunable 500 GHz transmitter array in SiGe technology for gas spectroscopy. *Electron Lett* 2015, 51:257–259.

77. Graf M, Barrettino D, Baltes HP, Hierlemann A. *CMOS Hotplate Chemical Microsensors*. Berlin and Heidelberg: Springer-Verlag; 2007.

78. Basmer T, Kulse P, Birkholz M. Systemarchitektur intelligenter Sensorimplantate. *Biomed. Eng./Biomed. Tech* 2010, 55:P43.

79. Johansson AJ. Performance of a radio link between a base station and a medical implant utilising the MICS standard. In: *Engineering in Medicine and Biology Society, 2004. IEMBS '04. 26th Annual International Conference of the IEEE*, San Francisco, CA, 2004, 2113–2116.

80. ETSI. Electromagnetic compatibility and Radio spectrum Matters (ERM); Short Range Devices (SRD); Ultra Low Power Active Medical Implants (ULP-AMI) and Peripherals (ULP-AMI-P) operating in the frequency range 402 MHz to 405 MHz; Part 1: Technical characteristics and test methods. *ETSI EN 301 839-1 V1.3.1 (2009-10)* 2010. Vol. ETSI EN 301 839-1 V1.3.1 (2009-10), 52 pp.

81. Basmer T, Genschow D, Fröhlich M, Birkholz M. Energy budget of an implantable glucose measurement system. *Biomed Tech/Biomed Eng* 2012, 57:259–262.

82. Birkholz M, Glogener P, Basmer T, Glös F, Genschow D, Welsch C, Ruff R, Hoffmann KP. System integration of a silicone-encapsulated glucose monitor implant. *Biomed Eng/Biomed Tech* 2014, 59(s1): S1089–S1092.

83. Dillschneider R, Posten C. Closed bioreactors as tools for microalgae production. In: Lee JW, ed. *Advanced Biofuels and Bioproducts*. New York: Springer; 2013, 629–649.

84. Todtenberg N, Basmer T, Klatt J, Schmalz K. Estimation of 433 MHz path loss in algae culture for biosensor capsule application. In: *European Microwave Conference (EuMC 2013)*. Nürnberg: IEEE; 2013, 712–715.

85. Todtenberg N, Schmitz-Hertzberg S-T, Schmalz K, Klatt J, Jorde F, Juttner B, Kraemer R. Autonomous sensor capsule for usage in bioreactors. *IEEE Sens J* 2015, 15:4093–4102.

86. Baratchi S, Khoshmanesh K, Sacristan C, Depoil D, Wlodkowic D, McIntyre P, Mitchell A. Immunology on chip: promises and opportunities. *Biotechnol Adv* 2014, 32:333–346.

87. Kling J. Moving diagnostics from the bench to the bedside. *Nat Biotechnol* 2006, 24:891–893.

88. Terry SC, Jerman JH, Angell JB. A gas chromatographic air analyzer fabricated on a silicon wafer. *IEEE Trans Electron Devic* 1979, 26:1880–1886.

89. Marschmeyer S, Fraschke M, Milewski T, Schulze S. Characterization of fluorocarbon polymers deposited with different chamber pressure and source power in

the deposition cycle of the Bosch process. In: *Plasma Etch and Strip in Microelectronics (PESM)*, Mechelen, Belgium, 2011.

90. Hwang T, Popa D, Sin J, Stephanou HE, Leonard EM. BCB wafer bonding for microfluidics. In: Maher MA, Jakubczak JF, eds. *Micromachining and Microfabrication Process Technology IX*. San Jose, CA: SPIE; 2004, 182–191.
91. Bauer J, Kulse P, Haak U, Kaynak M, Ehwald K-E, Marschmeyer S, Birkholz M, Schulz S, Old G, Scheuring G, et al. Alignment technology for backside integration. *Proc SPIE* 2011, 7985:798508.
92. Baristiran-Kaynak C, Kaynak M, Wietstruck M, Marschmeyer S, Kulse P, Schulz K, Silz H, Krüger A, Barth R, Schmalz K, et al. Modeling and characterization of BiCMOS embedded microfluidic platform for biosensing applications. *Silicon Monolithic Integrated Circuits in RF Systems*. Newport Beach, CA: IEEE; 2014, 46–48.
93. Kaynak M, Wietstruck M, Kaynak CB, Marschmeyer S, Kulse P, Schulz K, Silz H, Krüger A, Barth R, Schmalz K, et al. BiCMOS Integrated Microfluidic Platform for Bio-MEMS Applications. *International Microwave Symposium (IMS 2014)*, Tampa Bay, FL: IEEE; 2014.
94. Birkholz M, Ehwald K-E, Kaynak M, Semperowitsch T, Holz B, Nordhoff S. Separation of extremely miniaturized medical sensors by IR laser dicing. *J Opt Adv Mat* 2010, 12:479–483.

